AMINAHO, E.N. and HOSSAIN, M. 2023. *Caprock integrity evaluation for geosequestration of CO2 in low-temperature reservoirs*. Aberdeen: Robert Gordon University.

Caprock integrity evaluation for geosequestration of CO2 in low-temperature reservoirs.

AMINAHO, E.N. and HOSSAIN, M.

2023

This document was downloaded from
https://openair.rgu.ac.uk

CAPROCK INTEGRITY EVALUATION FOR GEOSEQUESTRATION OF CO_2 IN LOW TEMPERATURE RESERVOIRS

By

Principal Investigator:

Efenwengbe Nicholas Aminaho

1600684

Principal Supervisor:

Professor Mamdud Hossain

A project submitted to the Graduate School of Engineering in partial fulfillment of the requirements for the award of a Doctoral Degree in Petroleum Engineering at the Robert Gordon University

July 2023

ABSTRACT

The geological storage of CO_2, also referred to as CO_2 geosequestration, represents one of the most promising options for reducing greenhouse gases in the atmosphere. However, most of the time, CO_2 is captured and compressed together with small amounts of other industrial gases such as SO_2 and H_2S, incurring extra costs to separate these other acid gases before CO_2 storage in depleted petroleum reservoirs or aquifers. Moreover, during CO_2 geosequestration in reservoirs, pressure variations during injection could force some amount of CO_2 into the caprock, if the capillary entry or breakthrough pressure of the caprock is exceeded; thereby, altering the petrophysical, geochemical, and geomechanical properties of the caprock. Therefore, studies on the co-injection of CO_2 with other acid gases from industrial emissions and their impact on caprock integrity are paramount. In this study, numerical simulations were performed to investigate the co-injection of SO_2 and H_2S (separately) with CO_2 in carbonate and sandstone formations, and their migration to shale caprock. Furthermore, mathematical models were developed to evaluate the mineralogical brittleness index of the rocks, and compared with the mechanical brittleness index (which was evaluated using experimental data). The findings of the study indicate that SO_2 gas and H_2S gas dissolve preferentially in formation water compared with CO_2 gas, but SO_2 gas dissolves more rapidly than H_2S gas in formation water. Thus, the breakthrough of H_2S gas and SO_2 gas is delayed compared with CO_2 gas. CO_2-SO_2 and CO_2-H_2S separate co-injection cases result in the precipitation of pyrite through interactions between the dissolved gases (SO_2 and H_2S) and Fe^{2+} from the dissolution of iron-bearing minerals. However, no ankerite and siderite precipitations in the carbonate formations (only in the shale formation with a significantly higher concentration of Mg^{2+}) for the CO_2-H_2S case, but for the CO_2-SO_2 case ankerite and siderite precipitated in both the impure limestone and shale formations. Co-injection of SO_2 or H_2S with CO_2 inhibits the solubility trapping of CO_2 compared to the CO_2-only case. Furthermore, porosity and permeability increase for the CO_2 only and CO_2-H_2S injection cases, in both the carbonate and shale rocks; while for the CO_2-SO_2 injection case, porosity and permeability increase in the shale rock and carbonate rock (initially composed of calcite and dolomite) and decrease in the carbonate (pure and impure limestone) and sandstone rocks, due to anhydrite precipitation from the injection zone to the reservoir-caprock interface. In all the sequestration cases, the brittleness of the shale and sandstone rocks decreases, while the change in the brittleness of the carbonate rocks varies depending on calcite precipitation or dissolution. In comparison to the carbonate formations, shale formations are preferable as cap rocks, as their brittleness is low and decreases during CO_2 geosequestration; carbonate formations may be suitable reservoir rocks for cyclic injection and withdrawal of CO_2, due to increased injectivity and productivity in the injection and production zones, respectively; while sandstone formations are suitable for long-term storage of CO_2 (with or without impurities) due to their favourable mineral trapping of CO_2 and may also be suitable for cyclic injection of CO_2 (with or without H_2S impurity), except for cyclic CO_2 co-injection with high amount of SO_2 (which may decrease both injectivity and productivity of CO_2, due to reduced permeability and brittleness of the sandstone formation). Based on the mineralogical composition of the formations in this study, co-injection of H_2S gas and SO_2 gas (separately) with CO_2 gas, does not increase (but decreases) the brittleness of shale caprocks, as the brittleness is impacted mainly by the CO_2 gas.

TABLE OF CONTENTS

1.0 Introduction

Carbon dioxide (CO_2) geosequestration represents one of the most promising options for reducing atmospheric emissions of CO_2. It has been proposed as one solution to global climate change caused by heat-trapping of anthropogenic gases in the atmosphere (Wei et al., 2015; Klokov et al., 2017; Liu et al., 2020). What is fascinating about geosequestration is that CO_2 can be stored underground in caverns (salt cavern or engineered cavern) or porous media (aquifer and depleted oil or gas reservoirs). For long term storage of gases, underground storage in aquifer or depleted oil (or gas) reservoirs is preferrable due to high availability of aquifers and depleted oil or gas reservoirs in many part of the world.

CO_2 storage is possible by its different trapping mechanisms including residual trapping, solubility trapping, mineral trapping, and structural/stratigraphic trapping mechanisms (Sun et al., 2016). Residual trapping occurs as injected CO_2, which initially displaces the existing water (or brine) in the reservoir, gets displaced as the formation water imbibes back to the trailing edge of the CO_2 plume and trapping the gas in the form of isolated blobs. This trapping mechanism occurs relatively fast during CO_2 injection. As the injected CO_2 comes in contact with brine in the reservoir, some of it will dissolve into the formation water (solubility trapping). Thus, the fluid phase can no longer exist separately and the buoyant forces that drive it upwards is eliminated. After some time, the dissolved CO_2 in water lowers the initial brine pH (acidification of the groundwater) resulting in the fluid-rock interactions (chemical reactions) and leading to mineral trapping as the rock is made up of different minerals. This mineralization reaction begins after sometime during CO_2 injection and continues during the storage life of the porous rock, leading to dissolution and precipitation of minerals or aqueous complexes. During the period of CO_2 geosequestration, it is important to have a physical trapping which impedes the migration of CO_2 plume to the earth surface. It is a region or layer of porous media with a low-permeability seal and high capillary entry pressure, and caprock serves this purpose (Saraji et al., 2013; Edlmann et al., 2013; Sun et al., 2016). Nonetheless, caprock integrity ascertained based on its petrophysical, geochemical, and geomechanical properties is vital to ensure safe and sustainable storage of CO_2 (Pearce et al., 2016; Liu et al., 2020).

Caprock is any impermeable or low permeability formation that may trap gas, oil or water, preventing it from migrating to the surface (Klokov et al., 2017). Originally, most cap rocks have high mechanical strength, high stiffness, high capillary entry pressure, low compressibility, and very low permeability (Edlmann et al., 2013; Smith et al., 2009). However, during petroleum depletion as well as CO_2 injection and storage, caprock undergoes stresses and strains which impact its integrity. Hence, for long-term CO_2 storage, it is paramount to understand whether stress and strain changes caused by the gas injection or storage would lead to irreversible mechanical damages of the reservoir and impact the caprock integrity which could lead to CO_2 leakage through previously sealing structures (Li, 2016). Therefore, to properly evaluate caprock integrity. certain criteria based on rock theories of failure and rock mineral alterations, must be set to reflect changes in brittleness of reservoir and cap rocks.

During CO_2 injection and storage, the CO_2-brine-rock interaction results in dissolution and/or precipitation of minerals, which impacts the petrophysical and geomechanical properties of the rock. Due to the mineral alterations, the resulting change in mechanical properties of the minerals impact the brittleness of the rock. Thus, different concepts including fraction of reversible strain to total strain at rock failure (Hucka and Das, 1974; Hou et al., 2018; Li, 2022), brittleness based on rock strength parameters (Hucka and Das, 1974; Meng et al., 2015; Li, 2022), brittleness based on rock elastic parameters (Luan et al., 2014; Rickman et al., 2008; Kang et al., 2020), and brittleness based on mineralogical composition of the rock (Guo et al., 2016; Li, 2022) have been adopted to determine the brittleness of rocks. So, different studies have been conducted to investigate the impact of CO_2 geosequestration on the petrophysical, geochemical, and geomechanical properties of rocks.

Dissolution of primary minerals in carbonate rock increases the porosity and permeability of the rock (Wang et al., 2022, Sobia et al., 2021). Pure CO_2-brine-rock interaction results in increase in permeability of reservoir and caprock. Increase in permeability of reservoir and caprock was also observed in the case of co-injection of CO_2 and 100 ppm of H_2S. However, higher concentration of H_2S up to 5000 ppm in CO_2 decreased permeability of the reservoir and caprock (Bolourinejad and Herber, 2014). The permeability of the reservoir (sandstone) rock increases as 100 ppm of SO_2 was co-injected with CO_2, while permeability of the caprock changes by the carbonate to anhydrite composition ratio in the rock (Bolourinejad and Herber, 2014). Similarly, Aminu et al. (2018) found that CO_2 injection increases permeability, while CO_2 co-injection with H_2S or SO_2 decreases permeability (but higher permeability reduction with SO_2). Relatively significant decrease in permeability was observed with CO_2-NO_2-brine co-injection. These changes in permeability and porosity result from dissolution of these gases in water, thus reducing pH which enhances chemical reactions in the rock and result in dissolution of minerals (such as ankerite, siderite, dolomite, etc.), and precipitation of minerals (such as pyrite, dawnsonite, kaolinite, anhydrite, etc.) in the rock (Li et al., 2016; Pearce et al., 2016; Pearce et al., 2019).

Changes in the porosity of reservoir and cap rocks during CO_2 geosequestration are also impacted by the formation temperature and pressure. Davila et al. (2017) found that porosity of the caprock increases more under any partial pressure of CO_2 at lower temperature, while porosity reduced as temperature increased. Moreover, as partial pressure of CO_2 rises (increase in proportion of dissolved CO_2 in the formation water up to supercritical condition), porosity of the caprock enlarges over greater distances. Thus, the temperature of the system could have selective impact on dissolution and precipitation of minerals, and temperature is inversely related to porosity of the rock at the conditions considered. Therefore, dissolution or precipitation of minerals, and changes in porosity and permeability of a rock depend on the amount of impurities in the injected CO_2 stream, brine composition, lithology of the rock, formation temperature and pressure, and duration of CO_2 geosequestration.

AL-Ameri et al. (2014) and Tariq et al. (2018) studied the time-dependent effect of CO_2 geosequestration on the mechanical properties of rocks. Mechanical weakening of the rock increases with duration of CO_2 geosequestration. Alam et al. (2014) found that impact of supercritical CO_2 injection on geomechanical properties of chalk depends on the carbonate mineral content as rocks with high carbonate content experience significant mechanical weakening due to CO_2 injection, while rocks with low carbonate content experience negligible amount of mechanical weakening. In sandstone and shale rocks, Young's modulus, uniaxial compressive strength and Brazilian tensile strength decrease with co-injection of $scCO_2$ and brine (Huang et al., 2018; Lyu et al., 2018). But, the tensile fracturing behaviour of sandstone is not significantly affected by gaseous CO_2 in the presence or absence of water (Liu et al., 2014). Moreover, Masoudi et al. (2012) found that at low injection pressure (below 4200 psi), carbonate reservoir and cap rocks remain elastic despite a degradation of material elastic and strength properties, with increased CO_2 saturation and an increase in permeability up to 70% locally due to injection. Compactions induced during CO_2 production were fully recovered during the injection phase when the reservoir pressures were restored to their pre-production values. However, at high injection pressure, the rocks experience plastic deformation. Thus the rocks could fail over a certain amount of plastic deformation depending on the level of brittleness of the rocks. Lyu et al. (2018) found that intact CO_2-brine-shale interactions in shale sample decreases the brittleness values. The CO_2-brine solution has higher effect on the strength and Youngs modulus of the shale rocks than on the brittleness. Other studies did not consider impact of CO_2 injection on brittleness of rock, but developed models to determine brittleness of rocks based on weight fraction of the minerals (Kang et al., 2020), based on tensile brittleness index (Hou et al., 2018), and based on post-peak stress-strain curves under different confining pressure conditions (Meng et al., 2015).

Complex pressure variation exists in reservoirs during CO_2 injection and storage. During CO_2 injection, a slight increase in reservoir pore pressure or CO_2 injection pressure could result in reservoir fluid invasion into the caprock as soon as its capillary entry pressure is exceeded. CO_2 could also migrate into the caprock through diffusion, over a long period. Sadly, CO_2 streams contain some fraction of gas impurities such as H_2S or SO_2. Thus, as CO_2 penetrates the caprock, these gas impurities might continue to invade some of the caprock layers with the CO_2 by advective transport, until the injection pressure is reduced. Hence these invaded reservoir fluids become trapped in the caprock layers penetrated. The CO_2 mixture could alter the mineral composition of the rock, and consequently change the brittleness of the reservoir and cap rocks. If the brittleness of the caprock layers contacted by the CO_2 mixtures increases, it might become easier for the reservoir fluid to induce [tensile] fracture in the caprock layers with slight increase in the reservoir pore pressure during the period of CO_2 injection or storage. Otherwise, the caprock layers are able to handle higher amount of developed pressure during the period of CO_2 geosequestration. Therefore, identifying the impact of CO_2 mixtures on the brittleness of reservoir and cap rocks is paramount.

However, to properly evaluate the brittleness of reservoir and cap rocks, measurement of the changes in the mineralogical and mechanical changes of the rocks is required, as the changes in brittleness are controlled by alteration of the rock minerals and geomechanical properties. During CO_2 sequestration in depleted petroleum reservoir or aquifer, the rock experiences induced stresses as the fluid flows through interconnected pore spaces and the surrounding rock grains. The induced stresses developed lead to deformation and reduction in the strength (weakening) of the cement in rocks during CO_2 sequestration (Liu and Dai, 2021). Moreover, most times, CO_2 is captured with some other acid gases (such as H_2S and SO_2) and injected in reservoirs or aquifers. These acid gases might impact the reservoir and caprock integrity. To the best knowledge of the researcher, no study has been conducted to evaluate the impact of gas impurities in CO_2 on the brittleness of rocks. Hence, the aim of this study is to find out whether co-injection of CO_2 with some gas impurities impact the brittleness of reservoir and cap rocks. Specifically, this study investigates the impact of CO_2 impurities on porosity, permeability, and geochemical composition of reservoir and cap rocks; evaluates the impact of CO_2 impurities on the brittleness of reservoir and cap rocks during injection and storage of CO_2 stream; and determines best depleted reservoirs for CO_2 storage based on changes in the porosity, permeability, and brittleness of the reservoir rocks during CO_2 geosequestration.

2.0 Theoretical Framework

During CO_2 injection, stresses are induced in the rock as the cement that binds the rock grains are impacted. Thus, creating pathways for CO_2-brine-rock interaction in the [rock] cement and enhancing dissolution of some of its minerals. Hence, resulting in deformation and decrease in strength of the rock. The decrease in strength of the rock results in change in the brittleness of the rock, as the rate of decrease in the tensile and compressive strengths of the rock, as well as changes in the rock minerals are different. Brittleness is the lack of ductility or plasticity of a material, while ductility is the property of a material which allows it to be drawn out by tension to a smaller section (Hucka and Das, 1974; Hou et al., 2018). In other words, brittle materials can hardly be drawn into shapes. Instead, they fracture or break when such amount of stress is applied on them (Figure 1). Most rocks exhibit brittle behaviour. However, their degrees of brittleness vary by lithology and conditions subjected to during fluid-rock interactions.

Brittleness is a relative term as there are no accepted values of strength and elastic parameters ratios or brittle minerals ratio below which a material is considered brittle and above which it is considered as ductile (Hucka and Das, 1974). Brittleness of a material is compared by its brittleness index at one time or condition to another to ascertain whether the material has become more or less brittle. The factors that influence brittleness of rocks include internal geological and external environmental factors. According to Li (2022), the internal factors are the type and composition of brittle minerals, the content and maturity of organic matter, porosity, and rock bedding; while the external factors include temperature and confining pressure, which are influenced by burial depth and horizontal geostress differences.

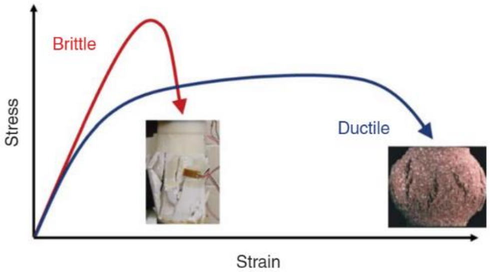

Figure 1: Stress-strain representation of brittle and ductile rocks (Jin et al., 2015)

During CO_2 injection, if the injection pressure or pore pressure slightly exceeds the capillary entry pressure of the caprock, CO_2 migrates into the caprock layers closer to the reservoir-caprock interface over a short time until the injection pressure is reduced. Therefore, it is important to investigate whether the CO_2 stream that penetrates the caprock impacts the rock brittleness. If the caprock layer penetrated becomes more brittle, during CO_2 storage a slight increase in the reservoir pore pressure will enhance advective CO_2 transport into the caprock or induce fracture. Otherwise, the caprock is able to contain the CO_2 and brine in the reservoir such that CO_2 can only penetrate the caprock layer by diffusion, which could take hundreds to thousands of years. To evaluate the brittleness of caprock penetrated by some amount of CO_2 during injection, in this section different methods for the evaluation of brittleness of a material are reviewed. Example of such methods or concepts are based on material deformation, strength and elastic parameters, and mineralogical composition of the rock.

2.1 Determination of brittleness from material deformation

The deformation based brittleness index is evaluated from the point of failure of the material. In this case, brittleness index is the ratio of reversible strain to total strain at the point of failure (Hucka and Das, 1974). In relation to Figure 2, OA represents the elastic limit, the stress at point B represents the peak strength (compressive or tensile strength) of the material, while C represents the point of failure.

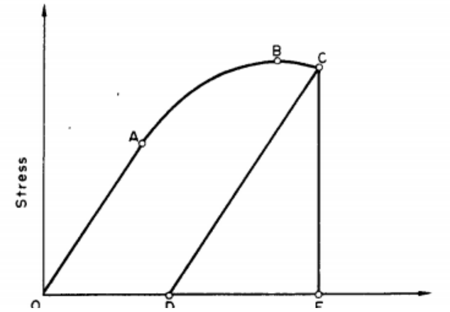

Figure 2: Stress-strain relationship to evaluate brittleness index

Based on this concept, ductile materials have lower brittleness index compared to brittle material. Thus, brittleness index (BI) is expressed in relation to Figure 2. as follows:

$$BI_1 = \frac{reversible\ strain}{total\ strain} = \frac{DE}{OE} \quad (1)$$

2.2 Determination of brittleness from strength parameters

It has been proposed that the brittleness index of a material depends on its compressive and tensile strength. The unconfined compressive strength reflects the compressibility of the rock mass, while the Brazilian tensile strength reflects the cohesion of the bonds between the material grains (Hucka and Das, 1974). It has been found that the ratio of compressive strength to tensile strength of a material increases with its brittleness (Meng et al., 2015; Li, 2022) . Similarly, some scholars have proposed that the difference in the tensile and compressive strength of a material increases with increase in brittleness index (Hucka and Das, 1974; Meng et al., 2015; Li, 2022). In other words, a rock mass with low [Brazilian] tensile strength is easily subjected to tensile fracture initiation and a high unconfined compressive strength assists in resisting the closure of natural and induced fractures (Gong and Zhao, 2007). Thus, brittleness index can be expressed as follows:

$$BI_2 = \frac{\sigma_c}{\sigma_t} \qquad (2)$$

$$BI_3 = \frac{(\sigma_c - \sigma_t)}{(\sigma_c + \sigma_t)} \qquad (3)$$

where σ_c represents uniaxial compressive strength and σ_t represents uniaxial tensile strength of the material .

2.3 Determination of brittleness from elastic parameters

Elastic parameters commonly used for brittleness index evaluation are Young's (or Elastic) modulus (E) and Poisson's ratio (ν). They can be obtained from destructive (static) or non-destructive (dynamic) testing of materials. Brittleness of a material increases with increase in the ratio of elastic modulus to Poisson's ratio (Luan et al., 2014). Although this estimation of brittleness has been criticized by some scholars, claiming that the brittleness of a material depends on several parameters such as bulk modulus and pore pressure (Zhang et al., 2016), it takes the lateral strain of the material into consideration such that under the same amount of axial strain, axial stress is proportion to lateral strain. Thus, when different materials are evaluated under the same amount of axial stress, the material that that is able to strain more laterally without failure is less brittle. Also, the brittleness of a material increases with increase in the average of normalized dynamic elastic modulus (E_n) and normalized dynamic Poisson's ratio (ν_n) for the formation investigated (Rickman et al., 2008; Kang et al., 2020). Therefore, brittleness index can be expressed as follows:

$$BI_4 = \frac{E}{v} \tag{4}$$

$$BI_5 = \frac{(E_n + v_n)}{2} = \frac{1}{2}\left[\frac{(E - E_{min})}{(E_{max} - E_{min})} + \frac{(v_{max} - v)}{(v_{max} - v_{min})}\right] \tag{5}$$

where E_{min} and E_{max} are the minimum and maximum dynamic Young's modulus for the investigated formation; v_{min} and v_{max} are the minimum and maximum dynamic Poisson's ratio for the investigated formation, respectively.

2.4 Determination of brittleness from rock mineralogical composition

During injection and storage of fluid in a porous rock, the pore fluid-rock interaction result in dissolution and precipitation of minerals (Edlmann et al., 2013; Sun et al., 2016). The brittleness of the rock depends on its lithology. For instance, shale is made up of mainly clay minerals and quartz with little amount of feldspar, calcite, pyrite, and other minerals (Guo et al., 2016); while carbonate rocks are made up of mainly calcite and little amount of other minerals (Wang et al., 2022). Brittle minerals are calcite, dolomite, feldspar (feldspar group of minerals), pyrite, mica (mica group of minerals, for example muscovite), and quartz (Jin et al., 2015; Guo et al., 2016; Li, 2022). So, the brittleness of a geomaterial or rock is the sum of the mass fraction of its brittlle minerals (Jin et al., 2015; Guo et al., 2016; Li, 2022). Therefore, brittleness index can be expressed as follows:

$$BI_6 = \frac{W_{quartz} + W_{feldspar} + W_{calcite} + W_{dolomite} + W_{pyrite} + W_{mica}}{W_T} \tag{6}$$

$$BI_7 = \frac{W_{quartz} + 0.49W_{feldspar} + 0.51W_{calcite} + 0.44W_{dolomite}}{W_T} \tag{7}$$

where W_T is the total mass of minerals in the solid part of the rock, and BI_7 is mineralogical brittleness index developed by Kang et al. (2020) based on the bulk modulus of brittle minerals.

During CO_2 geosequestration, CO_2-brine-rock interaction results in dissolution and precipitation of minerals; thus, the brittleness of the rock would vary over the geosequestration period as the volume fraction of the brittle minerals per rock [solid] volume changes. Mineralogical brittleness index correlates with the mechanical brittleness index to some extent (Kang et el., 2020). Therefore, it is possible that precipitation of more brittle minerals relative to their initial state before CO_2 geosequestration inhibits lateral strain on the rock when the same amount of axial stress is applied on the material, thus leading to a higher brittleness index of the rock. Dissolution of brittle minerals during CO_2 geosequestration in some cases can result in formation of non-brittle minerals. For instance, dissolution or corrosion of feldspar (potassium feldspar [$KAlSi_3O_8$], albite [$NaAlSi_3O_8$], etc.) as CO_2 dissolves in water (brine) might result in the precipitation of kaolinite [$Al_2Si_2O_5(OH)_4$], which is a clay mineral (Li et al., 2016) as shown below:

$$2KAlSi_3O_8 + 3H_2O + 2CO_2 \leftrightarrow Al_2Si_2O_5(OH)_4 + 2K^+ + 4SiO_2 + 2HCO_3^- \quad (8)$$

$$2NaAlSi_3O_8 + 3H_2O + 2CO_2 \leftrightarrow Al_2Si_2O_5(OH)_4 + 2Na^+ + 4SiO_2 + 2HCO_3^- \quad (9)$$

According to Li et al. (2016), with the co-injection of H_2S and CO_2 in the sandstone formation, the concentrations of K^+ and Na^+ increase, greater than those in pure CO_2 case. Thus, CO_2-H_2S co-injection enhances the corrosion or dissolution of feldspar, leading to the precipitation of larger amount of kaolinite compared to the case of pure CO_2. Also, pyrite (FeS_2) precipitated on the surface of the sandstone (Li et al., 2016). Studies have shown that residual or little amount of O_2 in the porous medium or presence of small minerals containing redox sensitive species (for example, Fe_2O_3) that has the tendency to dissolve and release oxidants to the brine could enhance SO_2 oxidation rate (Tursic et al., 2003; Hedayati et al., 2018). So, in the presence of residual O_2 in the porous medium, SO_2 (g) dissolves almost completely into the water (brine) quickly as SO_2 (aq), and oxidizes to sulphate under conditions controlled kinetically (Hedayati et al., 2018) giving rise to the following reaction:

$$SO_2\ (aq) + 0.5\ O_2\ (aq) + H_2O \rightarrow SO_4^{2-} + 2\ H^+ \quad (10)$$

Thus, in a porous medium where SO_2 is co-injected with CO_2, as the CO_2 plume rises [vertically] from the point of injection or perforation, SO_2 (g) might begin to dissolve quickly as SO_2 (aq) and oxidize to sulphate locally, limiting its ability to rise through different layers of the porous medium as SO_2 (g). Vertically, rise of the SO_2 (g) from the point of injection in the reservoir might be through very few metres in the porous medium. In the CO_2-SO_2 mixture, it is possible that supercritical CO_2 plume will rise relatively higher [or migrate laterally over a larger radial distance] in the porous medium as SO_2 oxidizes repidly to sulphate. Also, the difference in their relative vertical rise in the porous medium might be attributed to their density or molecular mass difference (as SO_2 is heavier than CO_2) due to gravity segregation (Khan and Mandal, 2020). Zhang et al. (2010) found the mass fraction of CO_2 at the advancing gas front to be higher (vertically) than that of the gas impurity. Thus, the front of the gas impurity behind that of CO_2 gas was attributed to the preferential solubility of the gas impurity in formation water compared to that of CO_2. This leads to delayed breakthrough of the gas impurity as the impurity separates from the CO_2 gas and [the impurity] becomes suppressed in formation water at the advancing gas front.

Furthermore, as dolomite dissolution in brine elevates Ca concentration, the increased Ca^{2+} reacts with the increased H_2SO_4 (due to enhanced sulphate concentration in the layers contacted by SO_2) to form anhydrite (Hedayati et al., 2018):

$$Ca^{2+} + H_2SO_4 \rightarrow CaSO_4 + 2H^+ \quad (11)$$

It is possible that as the molecular mass (and density) of CO_2 and H_2S is close, H_2S would correspondingly rise with the CO_2 plume in the porous medium. Thus, the injection of H_2S in the presence of oxygen and increased iron (Fe) concentration (due to the dissolution of siderite and/or ankerite) results in the precipitation of pyrite (Hedayati et al., 2018):

$$Fe^{+2} + 2H_2S + 0.5O_2 \rightarrow FeS_2 + H_2O + 2H^+ \quad (12)$$

Similarly, dissolved SO_2 (that oxidizes to sulphate) could result in the precipitation of pyrite as follows:

$$2Fe^{2+} + 4H^+ + 4SO_4^{2-} \rightarrow 2FeS_2 + 7O_2 + 2H_2O \quad (13)$$

Thus, it is possible that co-injection of gases (H_2S, SO_2, etc.) during CO_2 geosequestration impacts the brittleness of porous rocks as brittle and non-brittle minerals are precipitated during co-injection of CO_2 with different impurities. Therefore, it is vital to evaluate the impact of CO_2 impurities on the brittleness of rock during geosequestration.

3.0 Research Methodology

The research design involves mathematical modeling, numerical simulations, and laboratory scale experiments performed by AL-Ameri et al. (2016). The present study developed mathematical models for evaluation of brittleness index of rocks. Numerical simulations were performed by adopting two strategies: strategy 1 and strategy 2. Strategy 1 involves numerical simulations using pure limestone formation (as reservoir), impure limestone formation (to evaluate carbonate rock as a possible caprock), and shale caprock; while strategy 2 involves numerical simulations using sandstone and carbonate rocks as reservoirs [separately], and shale caprock. Results of the numerical simulations are analyzed using the developed models to evaluate brittleness of the rocks. The strength and elastic parameters from the experiment conducted by AL-Ameri et al. (2016) are analyzed to obtain mechanical brittleness index of the pure limestone (carbonate rock), which validates the mineralogical brittleness index evaluated using the developed mathematical models in the present study.

3.1 Governing Equations

Reactive transport in a porous medium result in the dissolution and/or precipitation of minerals under kinetic conditions or local equilibrium. Kinetic reactions of the minerals are based on rate law. Thus, the rate law relation is presented in this section. Also, new brittleness index models following the ratio of simple sum of brittle minerals to total minerals in rocks as well as brittleness index with respect to their relative level of brittleness based on their bulk modulus, using the concept of weight (or mass) fraction of minerals, is presented in this section.

3.1.1 Kinetic rate law for mineral dissolution and precipitation

Generally, the rate expression applied in TOUGHREACT is taken from Lasaga et al. (1994) and expressed as:

$$r_n = \pm k_n A_n \left[1 - \left(\frac{Q_n}{K_n}\right)^{\theta}\right]^{\eta} \qquad (14)$$

where η represents kinetic mineral index, k_n is the rate constant (in moles per unit mineral surface area and unit time) which is temperature-dependent, A_n denotes the specific reactive surface area per kilogram H_2O, K_n is the equilibrium constant for the mineral-water written for the destruction of one mole of mineral n, and Q_n is the reaction quotient. The parameters θ and η which are determined by experiments, are more often assumed to equal to one. Positive values of r_n indicate dissolution, while negative values indicate precipitation.

The kinetic rate constant (k) can be summed from three mechanisms for many minerals (Palandri and Kharaka, 2004) and expressed as:

$$k = k_{25}^{nu} exp\left[\frac{-E_a^{nu}}{R}\left(\frac{1}{T} - \frac{1}{298.15}\right)\right] + k_{25}^{H} exp\left[\frac{-E_a^{H}}{R}\left(\frac{1}{T} - \frac{1}{298.15}\right)\right] a_H^{n_H} + k_{25}^{OH} exp\left[\frac{-E_a^{OH}}{R}\left(\frac{1}{T} - \frac{1}{298.15}\right)\right] a_{OH}^{n_{OH}} \qquad (15)$$

where superscripts or subscripts nu, H, and OH indicate neutral, acid, and base mechanisms, respectively; E_a is the activation energy, k_{25} is the rate constant at 25^0C, R is the gas constant, T is the absolute temperature, α is the activity of the species, and n is an exponent (constant).

The rate constant (k) can also be dependent on other species such as Al^{3+} and Fe^{3+}. In fact, two or more species might be involved in one mechanism. Thus, a general form species-dependent rate constants implemented in TOUGHREACT is expressed as:

$$k = k_{25}^{nu} exp\left[\frac{-E_a^{nu}}{R}\left(\frac{1}{T} - \frac{1}{298.15}\right)\right] + \sum_i k_{25}^{i} exp\left[\frac{-E_a^{i}}{R}\left(\frac{1}{T} - \frac{1}{298.15}\right)\right] \prod_j a_{ij}^{n_{ij}} \qquad (16)$$

where superscripts or subscripts i represents the additional mechanism index, and j represents the species index involved in one mechanism that could be primary or secondary species. Currently, TOUGHREACT considers up to five additional mechanisms and up to five species involved in each mechanism (Zheng et al., 2009).

3.1.2 Petrophysical properties and derived mineralogical brittleness index equations

Change in porosity of the rock is calculated based on mineral precipitation and/or dissolution, while change in permeability is calculated from Carman-Kozeny relation, using the following equations (Xu et al., 2006; Xu et al., 2014):

$$\emptyset = 1 - \sum_{m=1}^{nm} fr_m - fr_u \qquad (17)$$

$$k = k_0 \left(\frac{1-\emptyset_0}{1-\emptyset}\right)^2 \left(\frac{\emptyset}{\emptyset_0}\right)^3 \qquad (18)$$

where, ϕ and k represent current porosity and permeability, ϕ_0 and k_0 represent initial porosity and permeability, parameters fr_m and fr_u represent volume fraction of mineral m in the rock (volume of mineral to volume of the medium including porosity) and volume fraction of non-reactive mineral, respectively. So, the output volume fraction of each mineral is the volume of mineral divided by volume of medium including porosity (V_{frac}). Thus, the volume of each mineral divided by total volume of solid [part of the rock] is calculated as follows (Xu et al., 2014):

$$f_m = \frac{V_{frac}}{1-\emptyset_{med}} \qquad (19)$$

where ϕ_{med} represents [current] porosity of the medium, and f_m represents the volume of mineral per volume of [the solid part of] the rock.

Mass fraction of composite materials has been calculated to determine their mechanical properties (Ezema et al., 2015) using their densities and volume fractions. Therefore, it is possible to determine the mass fraction of minerals in a rock using similar approach. Mass fraction of each material that forms a composite structure is the mass of that material to the total mass of materials that form the structure. Similarly, mass fraction of each mineral that forms a rock is the mass of each the individual mineral to the total mass of minerals that form the rock and can be expressed as follows:

$$Mass\ fraction\ of\ a\ mineral, x_i = \frac{mass\ of\ the\ mineral,}{total\ mass\ of\ minerals\ in\ the\ rock,} = \frac{m_i}{\sum_{i=1}^{nm} m_i} \quad (20)$$

$$m = V\rho \quad (21)$$

$$x_i = \frac{v_i \rho_i}{\sum_{i=1}^{nm} v_i \rho_i} \quad (22)$$

where V and ρ represent volume and density of solid, respectively; v_i represents volume fraction of each mineral in the solid part of the rock (same as f_m in Equation 3.6). Density can be expressed as molecular weight divided by molar volume.

$$\rho = \frac{\bar{M}}{\bar{V}} \quad (23)$$

Thus, mass fraction becomes:

$$x_i = \frac{\frac{v_i \bar{M}_i}{\bar{V}_i}}{\sum_{i=1}^{nm} \frac{v_i \bar{M}_i}{\bar{V}_i}} \quad (24)$$

where $\bar{M}$ and $\bar{V}$ represent molecular weight (g/mol) and molar volume (m^3/mol) of mineral. Hence, mineralogical brittleness index by simple sum of brittle minerals becomes:

$$BI = \frac{\sum_{j=1}^{nB} \frac{v_j \bar{M}_j}{\bar{V}_j}}{\sum_{i=1}^{nm} \frac{v_i \bar{M}_i}{\bar{V}_i}} \quad (25)$$

where j represents each brittle mineral in the rock, i represents any mineral in the rock, and nB represents the number of brittle minerals in the rock.

In the present study, to simplify the derived brittleness index equation, the same molar volume is assumed for all minerals. This is because the surface area of most of the minerals considered in this study is nearly the same except for some clay minerals such as smectite-Ca, smectite-Na, illite, and kaolinite which have larger mineral surface areas (Fatah et al., 2022) and possibly [significantly] different molar volumes. This assumption should not significantly impact the prediction of brittleness index in this study, as BI is a relative index and compares well as long as the rocks considered are under similar conditions. Thus, brittleness index in terms of simple sum of brittle minerals in a rock can be expressed as:

$$BI_8 = \frac{\sum_{j=1}^{nB} v_j \bar{M}_j}{\sum_{i=1}^{nm} v_i \bar{M}_i} \quad (26)$$

Brittle minerals considered in this study are quartz, feldspar (as albite, k-feldspar, oligoclase, and anorthite), calcite, dolomite, pyrite, and mica (as muscovite). Their relative level of brittleness among themselves (brittle minerals) are not considered in the simple sum of brittle minerals approach given above. Thus, to consider their relative level of brittleness, bulk modulus of the brittle minerals were incorporated into the equation following the mineralogical brittleness index developed by Kang et al. (2020). The mineralogical brittleness index, considering bulk modulus of minerals, developed by Kang et al. (2020) is given as:

$$BI_{BMod} = \frac{W_Q + 0.49W_F + 0.51W_C + 0.44W_D}{W_T} \tag{27}$$

where W_Q, W_F, W_C, and W_D represent the weights of quartz, feldspar, calcite, and dolomite, respectively; W_T represent the total mineral weight. The brittleness index in this case considers only quartz (Q), feldspar (F), calcite (C), and dolomite (D) as brittle minerals, assuming the level of brittleness of pyrite and mica is negligible compared to other brittle minerals. Thus, in the present study, brittleness index becomes:

$$BI = \frac{\frac{v_Q \bar{M}_Q}{\bar{V}_Q} + \frac{0.49 v_F \bar{M}_F}{\bar{V}_F} + \frac{0.51 v_C \bar{M}_C}{\bar{V}_C} + \frac{0.44 v_D \bar{M}_D}{\bar{V}_D}}{\sum_{i=1}^{nm} \frac{v_i \bar{M}_i}{\bar{V}_i}} \tag{28}$$

So, assuming the same molar volume of minerals in this present study, the brittleness index can be expressed as:

$$BI_9 = \frac{v_Q \bar{M}_Q + 0.49 v_F \bar{M}_F + 0.51 v_C \bar{M}_C + 0.44 v_D \bar{M}_D}{\sum_{i=1}^{nm} v_i \bar{M}_i} \tag{29}$$

Therefore, the models BI_8 and BI_9 developed in this study are used to evaluate the mineralogical brittleness index of the carbonate (pure limestone and impure limestone) and shale rocks before and after CO_2 geosequestration.

3.2 Numerical Approach

3.2.1 Numerical tool

This study employed the non-isothermal multiphase reactive geochemical transport code, TOUGHREACT (Xu et al., 2006), which is developed by incorporating reactive chemistry into the multiphase fluid and heat flow code TOUGH2 (Pruess, 2004). TOUGHREACT can be used to model the injection of CO_2 in saline formation and take into consideration the presence of additional gaseous species in the injected CO_2, such as H_2S and SO_2.

The numerical solution of fluid flow and chemical transport is based on an integral finite difference (IFD) method for space discretization (Narasimhan and Whiterspoon, 1976). The IFD method is flexible for the discretization of geologic media, as it can be adapted for irregular and regular grids. Thus, it is possible to simulate flow, transport, and fluid-rock interaction in heterogeneous or homogeneous rock systems with varying or similar petrology (Zhang et al., 2010). TOUGHREACT provides an implicit time-weighing scheme used for the flow, transport, and kinetic geochemical equations, and uses a sequential iteration approach similar to the model demonstration by Yeh and Tripathi (1991). Thus, after the solution of the flow equations, the velocities and saturations of the aqueous phase are used for aqueous chemical transport simulation. Then the chemical transport is solved on a component basis (Zhang et al., 2010). The concentration obtained from the transport as well as CO_2 and/or H_2S/SO_2 gas pressures in the multiphase flow calculation is substituted into the chemical reaction model. On a grid-block basis, the system of chemical reaction equations is solved by Newton-Raphson iteration. During mineral dissolution and/or precipitation, the porosity and permeability of the porous medium change, thereby modifying the fluid flow. Thus, feedback between flow and chemistry is considered in this model. Changes in porosity are calculated from rock volume changes due to mineral dissolution and/or precipitation. Then permeability changes are then evaluated by considering several alternative models that describe the porosity-permeability relationship, including the Kozeny-Carman relation, as used in this study.

3.2.2 Model setup

A simple two-dimensional (2-D) radial well model was used in this study. The 2-D model is a vertically heterogeneous formation of 40 m thickness with a cylindrical geometrical configuration (Figure 3). In the vertical direction, the model domain is discretized into 20 regular increments with a 2 m constant spacing (Δz). The top and bottom model boundaries are close to flow. The top model layers represent a shale caprock, while the remaining model layers at the bottom represent reservoir rock(s). The model layers for each strategy (strategies 1 and 2) are shown in Tables 1 and 2, respectively.

Table 1: Mesh generation of the model (Strategy 1).

Rock formation	Vertical mesh number	Mesh thickness (m)
Shale caprock	3	2.0
Impure limestone (carbonate)	3	2.0
Pure limestone (carbonate)	14	2.0

Table 2: Mesh generation of the model (Strategy 2).

Rock formation	Vertical mesh number	Mesh thickness (m)
Shale caprock	6	2.0
Carbonate or sandstone reservoir	14	2.0

In strategy 1, shale and impure limestone (carbonate) are examined as cap rocks, while pure limestone (carbonate) is examined as a reservoir formation. In strategy 2, carbonate (initially made up of calcite and dolomite minerals only) and sandstone formations are examined as reservoirs, and shale formation as caprock. In the horizontal direction, a 100 km radial distance was modeled with a radial grid spacing increasing logarithmically from the injection well. A total of 56 radial grid elements were generated. A large volume of 10^{30} m^3 is assigned to the outer grid element to represent an infinitive lateral boundary (a constant hydrostatic pressure boundary). CO_2 only (also referred to as CO_2 alone, in this study) or impure CO_2 (containing H_2S or SO_2) injection was applied at the bottom portion of the well in the reservoir. The thickness of the injection portion is 8 m, as shown in Figures 3 and 4.

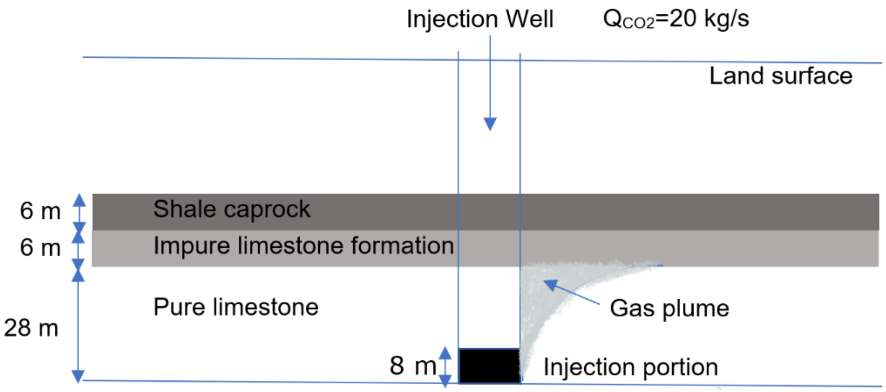

Figure 3: Strategy 1 - Schematic representation of the 2-D well flow model for the geosequestration of CO_2 in a carbonate formation (modified from Zhang et al., 2010).

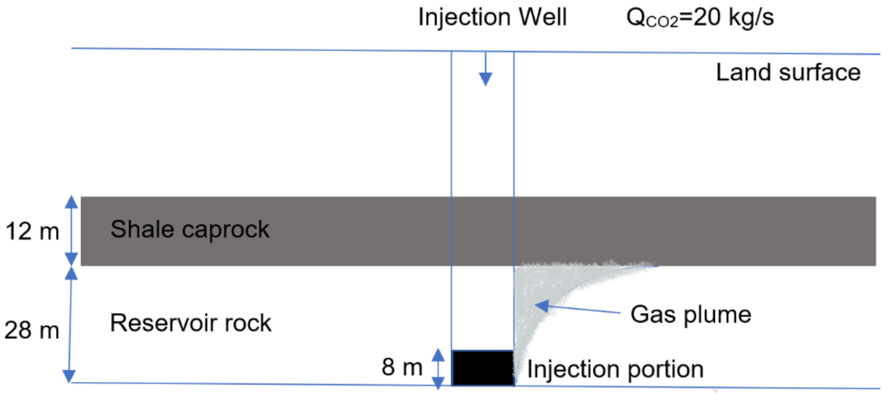

Figure 4: Strategy 2 – Schematic representation of the 2-D well flow model for the geosequestration of CO_2 in a reservoir (modified from Zhang et al., 2010).

In strategy 1, two simulation conditions were considered: injection into a high saline (salinity up to 0.21) formation at a pressure and temperature of 13.7 MPa (137 bar) and 100^{0}C, respectively; and injection into a low saline (salinity up to 0.06) formation at a pressure and temperature of 10 MPa (100 bar) and 40^{0}C (low-temperature condition), respectively. Injection of acid gases into the high saline reservoir was carried out for a period of 90 days, using a CO_2 injection rate of 20 kg/s (with or without a gas impurity) and with 0.025-mole fraction of H_2S or SO_2 (for the co-injection cases); while injection of acid gases into the low saline reservoir was applied for a period of 10 years, using a CO_2 injection rate of 20 kg/s (with or without a gas impurity) and with 0.025-mole fraction of H_2S or SO_2 (for the co-injection cases). The mole fraction of 0.025 for H_2S and SO_2 was selected as it is within the range of CO_2 co-capture from Pet Coke (SNC-Lavalin Inc., 2004). Similarly, in strategy 2, CO_2 is injected into the low salinity reservoir for a period of 10 years, at an injection rate of 20 kg/s (with or without a gas impurity) and with 0.025-mole fraction of H_2S or SO_2 (for the co-injection cases). The simulation of fluid flow and geochemical transport was run for a period of 100 years (strategies 1 and 2), which is a reasonable time scale for geosequestration of CO_2. It is worth noting that in the case of CO_2 co-injection with H_2S in the high saline formation, simulation was run only over the injection period (90 days) only, as the simulation did not progress beyond that period, possibly the high salinity and the reservoir temperature and pressure conditions were unfavourable for H_2S co-injection. The hydrogeological parameters used in this study are shown in Tables 3, 4, and 5.

Table 3: Hydrogeological parameters used in the simulation at formation temperature and pressure of 100^{0}C and 137 bar (Strategy 1), respectively.

Parameters	**Formation**		
	Pure limestone	**Impure limestone**	**Shale caprock**
Porosity	0.26	0.26	0.07
Horiizontal permeability (m^2)	2.264x10^{-12}	2.264x10^{-12}	2.264x10^{-17}
Vertical permeability (m^2)	2.264x10^{-13}	2.264x10^{-13}	2.264x10^{-18}
Pore compressibility (Pa^{-1})	2.10x10^{-9}	2.10x10^{-9}	2.10x10^{-9}
Rock grain density (kg/m^3)	2600	2600	2600
Formation heat conductivity (W/m ^{0}C)	2.51	2.51	2.51
Rock grain specific heat (J/kg ^{0}C)	920.0	920.0	920.0
Temperature (^{0}C)	100.0	100.0	100.0
Salinity (mass fraction)	0.21	0.21	0.21
Pressure (bar)	137	137	137
Gas saturation	0.00	0.00	0.00
CO_2 injection rate (kg/s)	20.0	-	-
Relative permeability Liquid: Van Genuchten function $k_{rl} = \sqrt{S^*}\left\{1 - \left(1 - [S^*]^{1/m}\right)^m\right\}^2$ S_{lr}: residual water saturation m: exponent Gas: Corey $k_{rg} = (1 - \widehat{S)}^2(1 - \hat{S}^2)$ S_{gr}: residual gas saturation	$S^* = (S_l - S_{lr})/(1 - S_{lr})$ $S_{lr} = 0.30$ $m = 0.457$ $\hat{S} = (S_l - S_{lr})/\left(1 - S_{lr} - S_{gr}\right)$ $S_{gr} = 0.05$		
Capillary pressure Van Genuchten function $P_{cap} = -P_0\left([S^*]^{-1/m} - 1\right)^{1-m}$ S_{lr}: residual water saturation m: exponent	$S^* = (S_l - S_{lr})/(1 - S_{lr})$ $S_{lr} = 0.03$ $m = 0.457$		
P_0: strength coefficient	19.61 kPa	19.61 kPa	19.61 kPa

Table 4: Hydrogeological parameters used in the simulation at formation temperature and pressure of 40^{0}C and 100 bar (Strategy 1), respectively.

Parameters	**Formation**		
	Pure limestone	**Impure limestone**	**Shale caprock**
Porosity	0.34	0.20	0.07
Horiizontal permeability (m^2)	2.264x10^{-12}	2.264x10^{-13}	2.264x10^{-16}
Vertical permeability (m^2)	2.264x10^{-13}	2.264x10^{-14}	2.264x10^{-17}
Pore compressibility (Pa^{-1})	2.10x10^{-9}	2.10x10^{-9}	2.10x10^{-9}
Rock grain density (kg/m^3)	2600	2600	2600
Formation heat conductivity (W/m ^{0}C)	2.51	2.51	2.51
Rock grain specific heat (J/kg ^{0}C)	920.0	920.0	920.0
Temperature (^{0}C)	40.0	40.0	40.0
Salinity (mass fraction)	0.06	0.06	0.06
Pressure (bar)	100	100	100
Gas saturation	0.00	0.00	0.00
CO_2 injection rate (kg/s)	20.0	-	-
Relative permeability Liquid: Van Genuchten function $k_{rl} = \sqrt{S^*}\left\{1 - \left(1 - [S^*]^{1/m}\right)^m\right\}^2$ S_{lr}: residual water saturation m: exponent Gas: Corey $k_{rg} = (1 - \widehat{S)}^2(1 - \hat{S}^2)$ S_{gr}: residual gas saturation	$S^* = (S_l - S_{lr})/(1 - S_{lr})$ $S_{lr} = 0.30$ $m = 0.457$ $\hat{S} = (S_l - S_{lr})/\left(1 - S_{lr} - S_{gr}\right)$ $S_{gr} = 0.05$		
Capillary pressure Van Genuchten function $P_{cap} = -P_0\left([S^*]^{-1/m} - 1\right)^{1-m}$ S_{lr}: residual water saturation m: exponent	$S^* = (S_l - S_{lr})/(1 - S_{lr})$ $S_{lr} = 0.03$ $m = 0.457$		
P_0: strength coefficient	19.61 kPa	19.61 kPa	19.61 kPa

Table 5: Hydrogeological parameters used in the simulation at formation temperature and pressure of 40^0C and 100 bar (strategy 2), respectively.

Parameters	**Formation**		
	Carbonate	**Sandstone**	**Shale caprock**
Porosity	0.34	0.34	0.07
Horiizontal permeability (m^2)	$2.264x10^{-12}$	$2.264x10^{-13}$	$2.264x10^{-16}$
Vertical permeability (m^2)	$2.264x10^{-13}$	$2.264x10^{-14}$	$2.264x10^{-17}$
Pore compressibility (Pa^{-1})	$2.10x10^{-9}$	$2.10x10^{-9}$	$2.10x10^{-9}$
Rock grain density (kg/m^3)	2600	2600	2600
Formation heat conductivity (W/m ^{0}C)	2.51	2.51	2.51
Rock grain specific heat (J/kg ^{0}C)	920.0	920.0	920.0
Temperature (^{0}C)	40.0	40.0	40.0
Salinity (mass fraction)	0.06	0.06	0.06
Pressure (bar)	100	100	100
Gas saturation	0.00	0.00	0.00
CO_2 injection rate (kg/s)	20.0	20.0	-
Relative permeability Liquid: Van Genuchten function $k_{rl} = \sqrt{S^*}\left\{1-\left(1-[S^*]^{1/m}\right)^m\right\}^2$ S_{lr}: residual water saturation m: exponent Gas: Corey $k_{rg} = (1-\widehat{S})^2(1-\hat{S}^2)$ S_{gr}: residual gas saturation	$S^* = (S_l - S_{lr})/(1-S_{lr})$ $S_{lr} = 0.30$ $m = 0.457$ $\hat{S} = (S_l - S_{lr})/\left(1-S_{lr}-S_{gr}\right)$ $S_{gr} = 0.05$		
Capillary pressure Van Genuchten function $P_{cap} = -P_0\left([S^*]^{-1/m}-1\right)^{1-m}$ S_{lr}: residual water saturation m: exponent	$S^* = (S_l - S_{lr})/(1-S_{lr})$ $S_{lr} = 0.03$ $m = 0.457$		
P_0: strength coefficient	19.61 kPa	19.61 kPa	19.61 kPa

Different types of [initial] mineralogical compositions were used. In strategy 1, carbonate (pure limestone) from AL-Ameri et al. (2016), modified carbonate (impure limestone) to account for impact of minor minerals in carbonate rocks, and shale modified from Ma et al. (2019); while sandstone and/or carbonate from Zhang et al. (2010), and shale modified from Ma et al. (2019) were used in strategy 2. The mineralogical compositions used in strategies 1 and 2 are shown in Tables 6 and 7, respectively.

Table 6: Initial mineral volume fractions and possible secondary minerals used in the simulations (strategy 1).

Mineral name	**Chemical formula**	**Molecular weight (g/mol)**	**Pure Limestone (volume percent of solid)**	**Impure Limestone (volume percent of solid)**	**Shale Caprock (volume percent of solid)**
Illite	$K_{0.6}Mg_{0.25}Al_{1.8}(Al_{0.5}Si_{3.5}O_{10})(OH)_2$	383.899	0	0.01	65.30
Kaolinite	$Al_2Si_2O_5(OH)$	258.159	0	0.01	1.11
Smectite-Ca	$Ca_{0.145}Mg_{0.26}Al_{1.77}Si_{3.97}O_{10}(OH)_2$	365.394	0	0.01	6.90
Chlorite	$Mg_{2.5}Fe_{2.5}Al_2Si_3O_{10}(OH)_8$	634.648	0	0.01	6.40
Quartz	SiO_2	60.084	0	0.01	8.00
K-feldspar	$KAlSi_3O_8$	278.33	0	0.01	2.80
Albite	$NaAlSi_3O_8$	262.222	0	0.01	3.20
Calcite	$CaCO_3$	100.087	100.00	99.91	0.83
Pyrite	FeS_2	119.98	0	0.01	0.40
Dolomite	$CaMg(CO_3)_2$	184.401	0	0.01	5.00
Anhydrite	$CaSO_4$	136.142	0	0	0
Alunite	$KAl_3(OH)_6(SO_4)_2$	414.214	0	0	0
Ankerite	$CaMg_{0.3}Fe_{0.7}(CO_3)_2$	206.48	0	0	0
Dawsonite	$NaAlCO_3(OH)_2$	143.995	0	0	0
Magnesite	$MgCO_3$	84.314	0	0	0
Siderite	$FeCO_3$	115.856	0	0	0
Smectite-Na	$Na_{0.290}Mg_{0.26}Al_{1.77}Si_{3.97}O_{10}(OH)_2$	366.25	0	0	0
Hematite	Fe_2O_3	159.692	0	0	0
Anorthite	$CaAl_2Si_2O_8$	278.206	0	0	0
Muscovite	$KAl_2(AlSi_3O_{10})(F,OH)_2$	398.306	0	0	0
Oligoclase	$CaNa_4Al_6Si_{14}O_{40}$	1327.094	0	0	0

Table 7: Initial mineral volume fractions and possible secondary minerals used in the simulations (strategy 2).

Mineral name	**Chemical formula**	**Molecular weight (g/mol)**	**Carbonate formation (volume percent of solid)**	**Sandstone formation (volume percent of solid)**	**Shale Caprock (volume percent of solid)**
Illite	$K_{0.6}Mg_{0.25}Al_{1.8}(Al_{0.5}Si_{3.5}O_{10})(OH)_2$	383.899	0	2.80	65.30
Kaolinite	$Al_2Si_2O_5(OH)$	258.159	0	0.90	1.11
Smectite-Ca	$Ca_{0.145}Mg_{0.26}Al_{1.77}Si_{3.97}O_{10}(OH)_2$	365.394	0	0	6.96
Chlorite	$Mg_{2.5}Fe_{2.5}Al_2Si_3O_{10}(OH)_8$	634.648	0	2.70	6.40
Quartz	SiO_2	60.084	0	25.80	8.00
K-feldspar	$KAlSi_3O_8$	278.33	0	23.30	2.80
Albite	$NaAlSi_3O_8$	262.222	0	41.50	3.20
Calcite	$CaCO_3$	100.087	40.00	3.00	0.80
Pyrite	FeS_2	119.98	0	0	1.43
Dolomite	$CaMg(CO_3)_2$	184.401	60.00	0	0
Anhydrite	$CaSO_4$	136.142	0	0	4.00
Siderite	$FeCO_3$	115.856	0	0	0
Alunite	$KAl_3(OH)_6(SO_4)_2$	414.214	0	0	0
Ankerite	$CaMg_{0.3}Fe_{0.7}(CO_3)_2$	206.48	0	0	0
Dawsonite	$NaAlCO_3(OH)_2$	143.995	0	0	0
Magnesite	$MgCO_3$	84.314	0	0	0
Smectite-Na	$Na_{0.290}Mg_{0.26}Al_{1.77}Si_{3.97}O_{10}(OH)_2$	366.25	0	0	0
Hematite	Fe_2O_3	159.692	0	0	0
Anorthite	$CaAl_2Si_2O_8$	278.206	0	0	0
Muscovite	$KAl_2(AlSi_3O_{10})(F,OH)_2$	398.306	0	0	0
Oligoclase	$CaNa_4Al_6Si_{14}O_{40}$	1327.094	0	0	0

Before the simulation of reactive transport, a batch geochemical modeling of water-rock interaction was performed to obtain an aqueous-phase chemical composition similar to the composition of a typical formation brine. So, synthetic brine formulated by AL-Ameri et al. (2016) with very little amount of other necessary ions based on the mineral compositions considered in the simulations was used. The synthetic brine was equilibrated separately for the different formations and injection conditions considered, in the presence of the primary minerals listed in Table 6 (strategy 1) and Table 7 (strategy 2). The batch geochemical modeling was conducted for 100 years to obtain a quasi-stable (or nearly steady-state) aqueous solution composition as shown in Tables 8 and 9 (strategy 1), and Table 10 (strategy 2).

Table 8: Initial concentrations of the formation water at formation conditions of 100^0C and 137 bars (strategy 1).

	Concentration (mol/kg H_2O)		
Component	**Pure limestone formation**	**Impure limestone formation**	**Shale caprock**
Ca^{2+}	4.7289E-01	4.6644E-01	3.4482E-01
Mg^{2+}	1.0034E-01	1.0489E-01	2.2812E-01
Na^+	2.5885E+00	2.5890E+00	2.5628E+00
K^+	1.9832E-10	2.6301E-03	1.1096E-02
Fe^{2+}	1.9861E-10	3.5599E-05	1.0361E-10
SiO_2 (aq)	1.9829E-10	3.7782E-03	2.6134E-03
HCO_3^-	3.6143E-03	2.3516E-03	6.5321E-05
SO_4^{2-}	3.6425E-03	3.6432E-03	3.6316E-03
AlO_2^-	1.9847E-10	2.4826E-09	1.0141E-08
Cl^-	3.7257E+00	3.7255E+00	3.7115E+00
pH	5.65	5.78	7.25

Table 9: Initial concentrations of the formation water at formation conditions of 40^0C and 100 bars (Strategy 1).

	Concentration (mol/kg H_2O)		
Component	**Pure limestone formation**	**Impure limestone formation**	**Shale caprock**
Ca^{2+}	4.7399E-01	4.6568E-01	9.0216E-03
Mg^{2+}	1.0036E-01	1.0693E-01	5.6313E-01
Na^+	2.5878E+00	2.5876E+00	2.5807E+00
K^+	1.9830E-10	4.9708E-04	2.6561E-03
Fe^{2+}	1.9835E-10	4.4246E-04	3.7561E-09
SiO_2 (aq)	1.9829E-10	1.3134E-03	1.7668E-03
HCO_3^-	4.6875E-03	2.9917E-03	5.8033E-03
SO_4^{2-}	3.6439E-03	3.6416E-03	3.6336E-03
AlO_2^-	1.9834E-10	1.7750E-10	4.0858E-11
Cl^-	3.7251E+00	3.7240E+00	3.7151E+00
pH	5.91	6.08	7.44

Table 10: Initial concentrations of the formation water at formation conditions of 40^{0}C and 100 bars (strategy 2).

Component	**Concentration (mol/kg H_2O)**		
	Carbonate formation	**Sandstone formation**	**Shale caprock**
Ca^{2+}	9.0400E-03	4.7137E-01	4.8163E-01
Mg^{2+}	5.6496E-01	1.0038E-01	9.7547E-02
Na^+	2.5814E+00	2.5868E+00	2.6006E+00
K^+	1.9781E-10	2.8166E-03	3.3113E-03
Fe^{2+}	1.9785E-10	4.9784E-04	2.7904E-08
SiO_2 (aq)	1.9782E-10	2.9555E-03	1.3991E-03
HCO_3^-	5.7553E-03	2.1733E-03	1.2688E-04
SO_4^{2-}	3.6350E-03	3.6425E-03	1.7486E-02
AlO_2^-	1.9782E-10	1.3611E-11	6.1835E-11
Cl^-	3.7158E+00	3.7245E+00	3.7264E+00
pH	7.4418	6.1989	7.3919

Dissolution and precipitation of minerals are considered under kinetic conditions based on the rate law, except calcite and anhydrite which are assumed to react with aqueous species at local equilibrium. This is because the reaction rates of calcite and anhydrite are typically quite rapid (Zheng et al., 2009). Most of the kinetic parameters were taken from Zhang et al. (2010) and shown in Table 11.

Table 11: List of parameters for calculating kinetic rate of minerals.

Mineral name	**Initial reactive surface area (cm^2/g)**	**Neutral mechanism**		**Acid mechanism**			**Base mechanism**		
		K_{25} (mol/m^2s)	**E_a (kJ/mol)**	**K_{25} (mol/m^2s)**	**E_a (kJ/mol)**	**$n(H^+)$**	**K_{25} (mol/m^2s)**	**E_a (kJ/mol)**	**$n(H^+)$**
Calcite	Assumed in equilibrium								
Anhydrite	Assumed in equilibrium								
Quartz	9.8	1.0233E-14	87.7						
Kaolinite	151.63	6.9183E-14	22.2	4.8978E-12	65.90	0.777	8.9125E-18	17.90	-0.472
Illite	151.63	1.6596E-13	35.00	1.0471E-11	23.6	0.34	3.02E-17	58.9	-0.40
Pyrite	12.87	2.8184E-05	56.90 $n_{O2(aq)}$=0.5	3.02E-08	56.9	n_{H+}=-0.5 n_{Fe3+}=0.5			
K-feldspar	9.8	3.8905E-13	38.0	8.7096E-11	51.7	0.5	6.3096E-22	94.1	-0.823
Dolomite	9.8	2.9512E-08	52.20	6.4565E-04	36.1	0.5			
Siderite	9.8	1.2598E-09	62.76	6.4565E-04	36.1	0.5			
Ankerite	9.8	1.2598E-09	62.76	6.4565E-04	36.1	0.5			
Albite	9.8	2.7542E-13	69.80	6.9183E-11	65.0	0.457	2.5119E-16	71.0	-0.572
Muscovite	9.8	3.160E-13	58.6						
Hematite	12.87	2.5119E-15	66.2	4.0738E-10	66.2	1.0			
Chlorite	9.8	3.020E-13	88.0	7.7624E-12	88.0	0.5			
Oligoclase	9.8	1.4454E-13	69.8	2.1380E-11	65.0	0.457			
Magnesite	9.8	4.5709E-10	23.5	4.1687E-07	14.4	1.0			
Dawsonite	9.8	1.2598E-09	62.76	6.4565E-04	36.1	0.5			
Smectite-Na	151.63	1.6596E-13	35.0	1.0471E-11	23.6	0.34	3.0200E-17	58.9	-0.40
Smectite-Ca	151.63	1.6596E-13	35.0	1.0471E-11	23.6	0.34	3.0200E-17	58.9	-0.40
Alunite	9.8	1.0000E-12	57.78				1.0000E-12	7.5	-1.00
Anorthite	9.8	1.5000E-14	18.4						

A temperature of 100^{0}C was used in the high saline reservoir which may represent the temperature at a depth of about 2800 m, given a land surface temperature of 16^{0}C and a geothermal gradient of 30^{0}C/km; while a temperature of 40^{0}C was used in the low saline reservoir which may represent shallow formation temperature at a depth of about 800 m, given a land surface temperature of 16^{0}C and a geothermal gradient of 30^{0}C/km. The temperature in the reservoir and cap rocks are assumed to be initially the same as the rock thickness considered in the simulation is only 40 m. Also, the numerical simulations are conducted under isothermal condition.

3.2.3 Simulations

Six (6) groups of numerical simulations were performed in strategies 1 and 2, with different combinations of injection and formation conditions as shown in Tables 12 and 13, respectively. The objective is to investigate the effect of CO_2 injection or CO_2 co-injection with other gases (H_2S or SO_2) on the petrophysical (porosity and permeability) and geochemical (aqueous composition and mineral dissolution/precipitation) changes of the rocks, and evaluate the brittleness of the rocks during CO_2 geosequestration.

Table 12: Six groups of simulations in this study (strategy 1).

Simulation groups	Injection scenarios	Formation	Formation salinity
1	CO_2 only	Carbonate and shale	0.21
2	CO_2 and H_2S	Carbonate and shale	0.21
3	CO_2 and SO_2	Carbonate and shale	0.21
4	CO_2 only	Carbonate and shale	0.06
5	CO_2 and H_2S	Carbonate and shale	0.06
6	CO_2 and SO_2	Carbonate and shale	0.06

Tables13: Six groups of simulations in this study (strategy 2).

Simulation groups	Injection scenarios	Formation	Formation salinity
1	CO_2 only	Carbonate and shale	0.06
2	CO_2 and H_2S	Carbonate and shale	0.06
3	CO_2 and SO_2	Carbonate and shale	0.06
4	CO_2 only	Sandstone and shale	0.06
5	CO_2 and H_2S	Sandstone and shale	0.06
6	CO_2 and SO_2	Sandstone and shale	0.06

3.3 Model Validation

The numerical simulations performed in this study were validated using experimental results from a study conducted by AL-Ameri et al. (2016) to determine the long-term effects of CO_2 sequestration on rock mechanical properties. The rock sample, from AL-Ameri et al. (2016), relevant for the present study is the Pink Desert limestone (PL). The porosity of the rock samples are shown in Table 14, indicating an average porosity of 26% for the carbonate rocks in strategy 1. The X-ray diffraction (XRD) was used to determine the mineral composition of the carbonate samples, which is shown in Table 15.

Table 14: Basic core properties

Sample ID	Brine porosity (%)
PL-S-1-A	26.067
PL-S-2-A	27.792
PL-S-3-B	28.745
PL-U-1-A	26.022
PL-U-2-A	25.680
PL-U-3-B	26.652
PL-T-1-A	26.740
PL-T-1-B	26.332
PL-T-2-A	26.634
PL-T-3-C	26.005

Table 15: Quantitative analysis of the core samples using XRD

Sample name	Phase name	Content (%)
Pink Desert limestone (PL)	Calcite Quartz	100 0

The purity of CO_2 used in the study was 99%, to minimize the chance of introducing contaminants in the rock samples. The composition of the brine used in the study is shown in Table 16. The total dissolved solids (TDS) of the brine was 213,734 ppm (about 0.21 salinity). The system temperature and pressure during the CO_2 sequestration experiments were 100^{0}C and 2000 psi (~ 137 bar), respectively. Destructive tests including unconfined compressive tests and Brazilian tensile tests were conducted to determine Young's modulus, Poisson's ratio, and peak strengths (uniaxial compressive strength [UCS] and indirect tensile strength [ITS]) of the rock samples before and after CO_2 storage. Results of the experiments are shown in Table 17.

Table 16: Ionic composition of the brine

Ions	Composition (ppm)
Sodium	59,491
Calcium	19,040
Magnesium	2439
Sulfate	350
Chloride	132060
Carbonate	0
Bicarbonate	354
TDS	213734

Table 17: Mechanical properties of the PL core samples before and after CO_2 sequestration

Rock mechanical properties	Before CO_2 sequestration	After CO_2 sequestration (90 days)
Indirect tensile strength (psi) (MPa)	199.137 1.373	142.8 0.9846
Uniaxial compressive strength (MPa)	17.0	12.4
Static Young's modulus (GPa)	16.18	14.0
Static Poisson's ratio	0.353	0.233

The impact of impurities on the brittleness of rocks is validated using experimental results published by Mavhengere et al. (2022) on the influences of SO_2 contamination in long term supercritical CO_2 treatment on the physical and structural characteristics of sandstone rock. They conducted two types of storage experiments on sandstone core samples (Cenomanian Sandstone, ZG and Siltstone lateral seal Aptian Sandstone, ZC) from Zululand Basin in South Africa, using pure CO_2 gas (purity of 99.9% by weight); and another case using a mixture of 99% (weight) CO_2 and 1% (weight) SO_2 gas. Non-stirred Teflon lined N4766 Parr reactors were used to simulate geosequestration conditions of 17.5 MPa and 346 K for the ZC core samples, and 10 MPa and 316K for the ZG core samples for 2 months. XRD analyses were conducted on the samples before and after treatment with CO_2 or CO_2-SO_2 mixture to investigate any mineral phase alterations. The ZC core sample exhibited mineral phase alteration after treatment (fluid-rock interaction) similar to the sandstone rock in the present study. Therefore, to validate the mathematical models developed to evaluate the impact of contaminant (SO_2) in CO_2 on brittleness index of sandstone, the mineral phases (weight fraction) of the ZC core samples (shown in Table 18) was incorporated into existing models that are based on simple weight fraction of brittle minerals (Jin et al., 2015; Guo et al., 2016; Li, 2022) and weight fraction considering the relative brittleness of brittle minerals (Kang et al., 2020). In this case, the brittle minerals are quartz, plagioclase (feldspar), calcite, pyrite, and orthoclase (feldspar).

Table 18: ZC and ZG core samples XRD results before and after $ScCO_2$-water and $ScCO_2$-SO_2-water treatment (Source: Mavhengere et al., 2022)

Sample	**Quartz (wt. %)**	**Plagioclase (wt. %)**	**Smectite (wt. %)**	**Calcite (wt. %)**	**Pyrite (wt. %)**	**Stilbite (wt. %)**	**Diopside (wt. %)**	**Gypsum (wt. %)**	**Orthoclase (wt. %)**
ZC untreacted	44.1	44.7	1.0	3.5	0.4	3.6	2.7	0.0	0.0
ZC CO_2 treated	47.5	42.5	2.5	1.7	0.4	2.7	2.8	0.0	0.0
ZC CO_2-SO_2 treated	49.1	28.6	11.8	0.0	0.8	4.9	2.3	2.5	0.0
ZG untreacted	21.5	46.0	22.2	0.0	0.0	2.0	0.0	0.0	8.3
ZG CO_2 treated	22.3	50.5	16.3	2.9	0.0	4.8	0.0	0.0	3.2
ZG CO_2-SO_2 treated	26.1	53.4	12.1	2.3	0.0	0.0	0.0	0.0	6.2

3.4 Data Analysis Techniques

Numerical simulations were analyzed for changes in petrophysical and geochemical properties of reservoir and cap rocks, to investigate the impact of CO_2 mixtures on those properties. In addition, data from the experiment (AL-Ameri et al., 2016) were analyzed to determine the mechanical brittleness index of the rock, using equations of elastic and strength parameters; while the mineralogical brittleness index was calculated from the models developed in the present study. The calculated mechanical brittleness indices were compared with the mineralogical brittleness indices for the high saline formations injected with CO_2 only.

Furthermore, mineralogical brittleness indices were calculated for simulation groups of CO_2 co-injection with another gas (H_2S or SO_2) into the reservoir and advective [and diffusive] transport into the caprock layers, to determine the impact of CO_2 mixtures on the brittleness of reservoir and cap rocks in high or low salinity conditions. The results from the analyses are validated with experimental data published by Mavhengere et al., (2022) and are presented in tables and graphs for proper visualization and comparison. It is worth noting that while discussing the results of the analyses, the expression “SO_2 (or H_2S) gas co-injection with CO_2” or “SO_2/H_2S gas co-injection with CO_2” implies that SO_2 co-injection with CO_2 is one case, and H_2S co-injection with CO_2 is another case in the numerical simulations.

4.0 Results and Discussions

4.1 Results

4.1.1 Impact of impurities on porosity, permeability, and geochemical composition of reservoir and cap rocks during CO_2 injection, withdrawal and storage (Strategy 1)

The supercritical CO_2 fluid (referred to as ‘gas’ in this study for simplicity) is injected or co-injected with H_2S (or SO_2) near the bottom of the pure limestone (carbonate reservoir). The injected fluid migrates rapidly upward by buoyant forces, as the density of the supercritical CO_2 phase is less than that of the aqueous phase or formation water (Figure 5). After the period of injection, a small fraction of CO_2 gas is trapped in the pure and impure limestone porous rocks as residual gas. The mobile gas continues to migrate into the shale caprock by the action of buoyant forces. At the same time, some amount of the gas continues to dissolve into brine (formation water) and precipitate carbonate minerals. Hence, the residual gas slowly disappears at the bottom of the pure limestone reservoir.

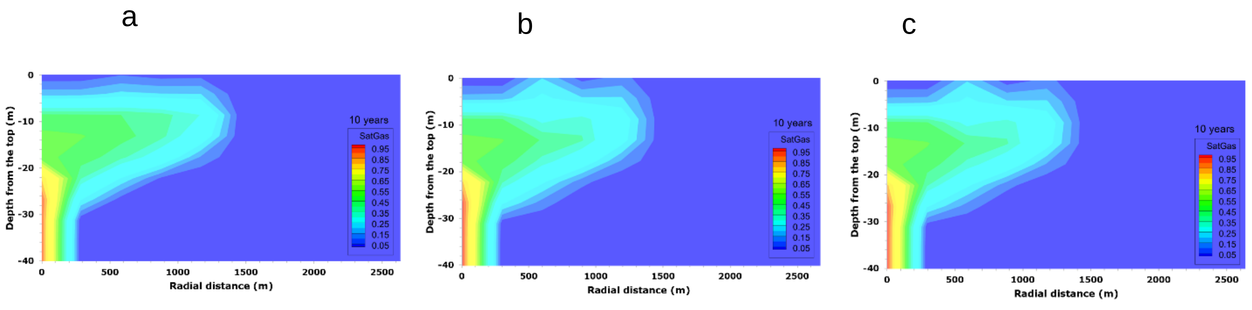

Figure 5: Gas saturation (a) CO_2 alone (b) CO_2-H_2S (c) CO_2-SO_2 case.

After some time, most of the free CO_2 gas accumulates in the shale caprock layers, few metres from the reservoir-caprock interface, and spreads laterally. At 10 years of injection, reservoir rock pores are majorly filled with free CO_2 gas up to radial distance of 15 m (water nearly drying out in the zone). In fact, the higher gas saturation in the rock pores near the injection well extends over a longer radial distance in the CO_2 and H_2S/SO_2 co-injection cases compared to the CO_2 alone case, as shown in Figure 5. However, after injection (10 years), formation water re-invades the zones where water was nearly dried out, enabling chemical reactions (dissolution and precipitation) between the dissolved CO_2 and minerals.

The front of H_2S (or SO_2) gas are behind that of CO_2 gas (Figure 6). This is due to the preferential solubility of H_2S and SO_2 in formation water compared to that of CO_2. Thus, delayed breakthrough of H_2S (or SO_2) gas is experienced, and H_2S (or SO_2) gas begins to separate from the CO_2 gas (in the gas mixture), and H_2S (or SO_2) concentration in the formation water at the advancing gas front gets suppressed. This situation is more severe with SO_2 gas compared to H_2S gas. The front of SO_2 gas is far behind that of CO_2 gas compare to the front of H_2S gas with respect to CO_2 gas as shown in Figure 6. Hence, the solubility of SO_2 gas in formation water is higher than that of H_2S and CO_2. In fact, the solubility of SO_2 gas in water at a higher formation salinity (0.21) and temperature (100^{0}C) increases, resulting in complete dissolution of SO_2 in formation water after 100 years of CO_2 geosequestration as shown in Figure 7.

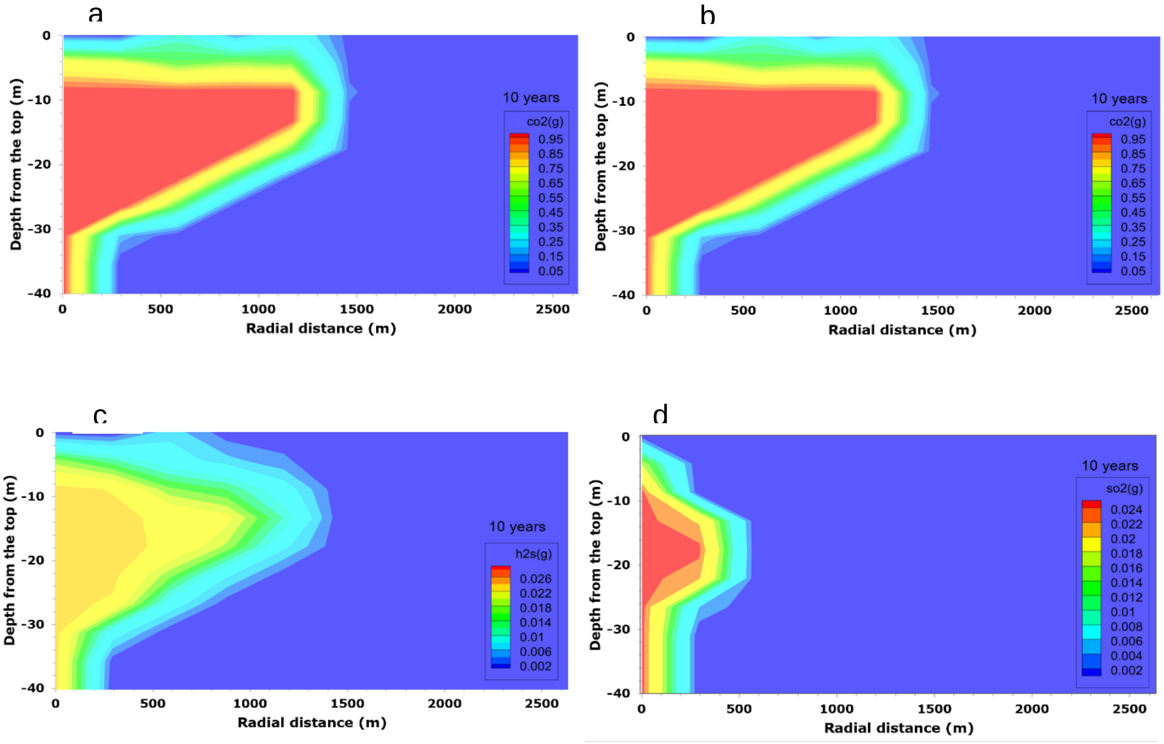

Figure 6: Gas front of (a) CO_2 in CO_2-H_2S(b) CO_2 in CO_2-SO_2 (c) H_2S (d) SO_2.

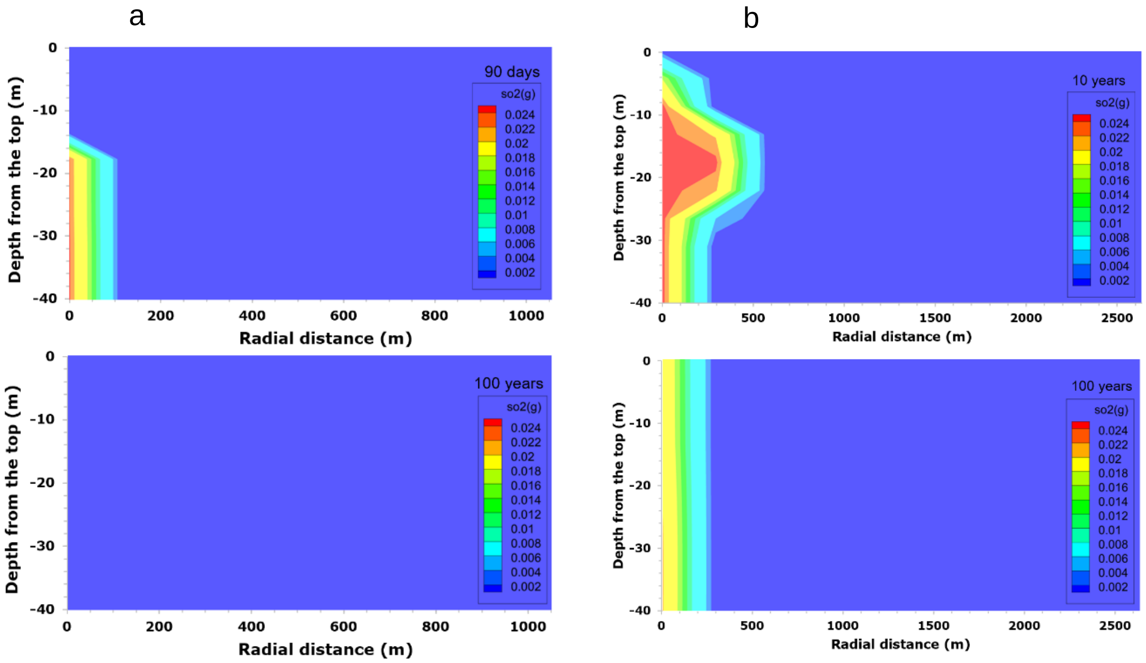

Figure 7: SO_2 gas mole fraction after CO_2 co-injection and 100 years of sequestration (a) at 100^{0}C and 137 bar (b) at 40^{0}C and 100 bar.

Figure 8 shows the spatial distribution of total dissolved carbon (TDC) in the rocks. CO_2 mobilises faster than H_2S (or SO_2). This is due to the preferential dissolution of H_2S and SO_2 compared with CO_2. The concentration of total dissolved carbon at the advancing front increases as the concentration of H_2S (or SO_2) gas has been suppressed in the formation water. Moreover, the concentration of TDC in the co-injection cases is lower than that in the CO_2 alone case. This implies that the preferential dissolution of H_2S (or SO_2) gas reduces the potential and capacity for the dissolution of the injected CO_2 gas in formation water (Zhang et al., 2010).

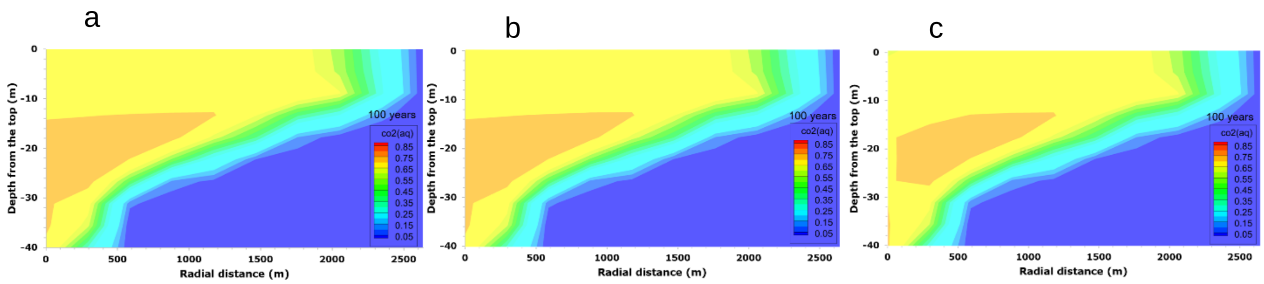

Figure 8: Total dissolved carbon for (a) CO_2 alone case (b) CO_2-H_2S case (c) CO_2-SO_2 case

The total dissolved CO_2 concentrations after 100 years of geosequestration are shown in Figure 8. The concentration of dissolved CO_2 increases to over 0.6 mol/kg H_2O in the two-phase region due to the CO_2 gas migration. The dissolution of the injected CO_2 (with or without cases of H_2S or SO_2 gas co-injection) in the surrounding formation water yields H_2CO_3, HCO_3^-, and CO_3^{2-}, and decreases pH (increases acidity). The pH profiles of all the injection cases are similar, as shown in Figure 9.

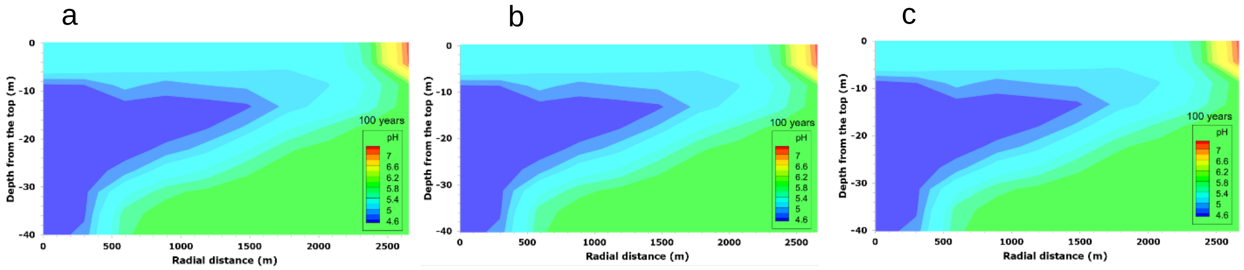

Figure 9: pH for (a) CO_2 alone (b) CO_2-H_2S (c) CO_2-SO_2 co-injection case.

The low pH induces the dissolution and precipitation of minerals. Dissolution of the minerals increases concentrations of cations including Na^+, Ca^{2+}, Mg^{2+}, and Fe^{2+}, which then form aqueous complexes with the carbonate ions and further precipitation of minerals (including secondary minerals). Example of such aqueous complexes are $NaHCO_3$, $CaHCO_3^+$, $MgHCO_3^+$, and $FeHCO_3^+$; and example of precipitated secondary minerals are ankerite, dawsonite, magnesite, siderite, smectite-Na, and anhydrite (CO_2-SO_2 co-injection case). As the aqueous complexes are formed, more CO_2 goes into solution and enhance solubility trapping. However, mineral trapping of CO_2 was not considered in this study as it is a slow process that occurs over hundreds to thousands of years, while the numerical simulations in the present study were performed up to a maximum of 100 years. So, the CO_2 trapping mechanisms in the present study are structural/stratigraphic trapping (caprock), residual trapping, and solubility trapping. During the CO_2 injection period (up to 10 years), out of a total of about 6.31 M ton of CO_2 injected, a large amount of injected CO_2 remains as a free supercritical phase. After injection, some amount of CO_2 dissolved in the formation water gradually, while the injected gas plume continues to migrate upward and horizontally. In fact, Convective mixing between CO_2-saturated water and unsaturated water also takes place at the same time. After 100 years of sequestration, 69% of the injected CO_2 is stored in the gas phase, while the remaining 31% is stored in the aqueous phase (since mineral trapping was nost considered in the present study).

Generally, minerals such as chlorite, albite, dolomite, and k-feldspar in the shale and impure limestone formations dissolve in the two-phase region and near the front of the single aqueous-phase zone. On the other hand, quartz, illite, smectite-Ca, and smectite-Na precipitated in those zones. Other minerals exhibited selective dissolution or precipitation in different formations. It is worth noting that due to fluid-rock interaction between zones with different lithology, minerals such as quartz and smectite-Na precipitated in some layers of the pure limestone formation (which would not have been possible without upward and downward (vertical) flow of fluids from different rock layers). After 100 years of CO_2 only sequestration, minerals such as ankerite, magnesite, pyrite, and calcite (due to higher pH in the region) precipitated in the shale caprock; while kaolinite dissolution was observed in the formation. On the other hand, kaolinite, dawsonite, ankerite and small amount of magnesite and siderite precipitated in the impure limestone formation; while pyrite and calcite dissolution was observed in the impure limestone formation. In the pure limestone reservoir, calcite dissolution was observed throughout the period of sequestration. Changes in the composition (volume fraction of the solid rock) of some of the minerals in the CO_2 alone sequestration case is shown in Figure 10.

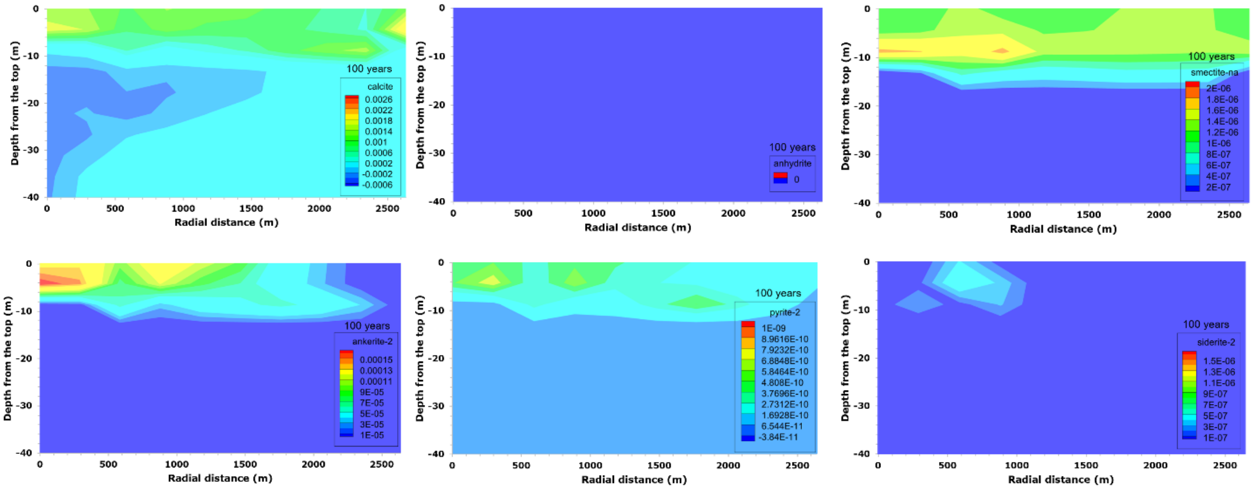

Figure 10: Some minerals in the formations for the CO_2 alone case.

The same kind of mineral precipitation and dissolution was observed in the co-injection cases, except that in the case of H_2S co-injection with CO_2, no ankerite and siderite precipitation. Little amount of ankerite was observed in the shale caprock only in the region where dissolved H_2S in formation water is low in concentration (Figure 11). But pyrite precipitation was observed in all the formations considered, in all the regions where H_2S dissolved in the formation water. This is because precipitation of siderite and ankerite requires Fe^{2+} which can be supplied by the dissolution of iron-bearing minerals such as chlorite. Furthermore, in the case of SO_2 co-injection with CO_2, after 100 years of sequestration, ankerite, and magnesite precipitated in the shale caprock, while anhydrite and pyrite precipitated in the carbonate rocks in the region where SO_2 gas has dissolved in formation water (Figure 12). Beyond this region, ankerite, siderite, and magnesite precipitation were observed. Precipitation of pyrite reduces ankerite precipitation (Zhang et al., 2010). Overall, the mineral precipitation and dissolution are the same at temperatures of 40^0C (as analysed above) and 100^0C. the only difference is that calcite precipitated in the shale and impure limestone formations in the case of CO_2 alone sequestration.

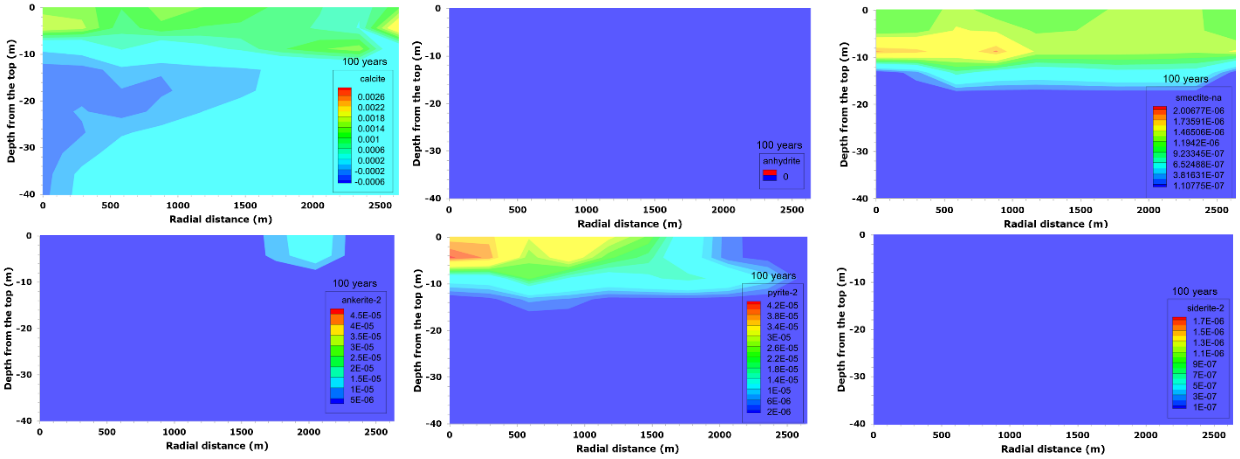

Figure 11: Some minerals in the formations for the CO_2-H_2S co-injection case.

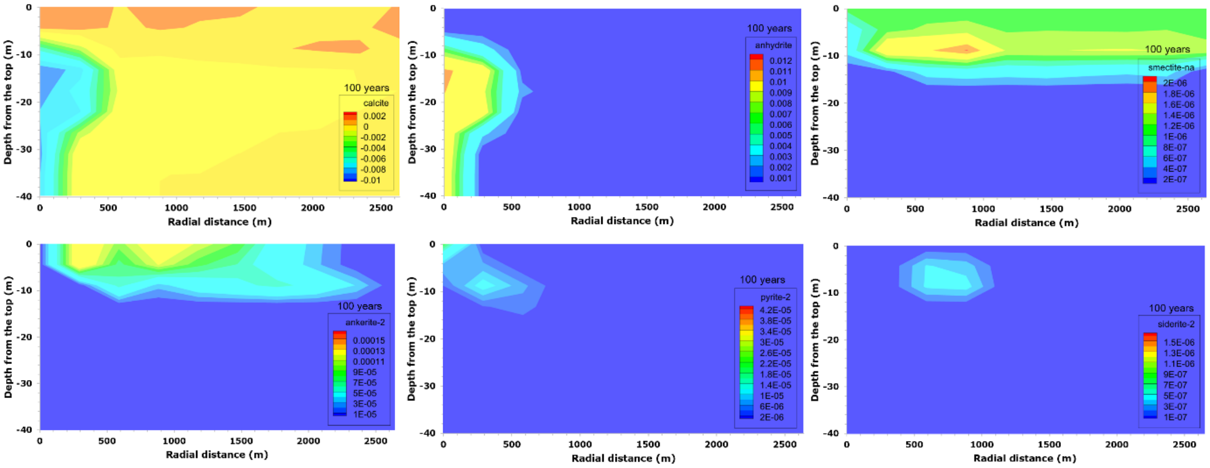

Figure 12: Some minerals in the formations for the CO_2-SO_2 co-injection case

Changes in porosity are calculated from variations in the volume fraction of the minerals and presented in Table 19 and Figure 13. In the two-phase region, due to dominant mineral dissolution caused by low pH, porosity increases slightly in the shale and carbonate rocks, in the case of CO_2 alone and CO_2-H_2S co-injection, while in the case of CO_2-SO_2 co-injection, porosity increases only in the shale rock, and decreases in the carbonate rocks due to anhydrite precipitation. Outside the regions where SO_2 dissolved in the formation water in the carbonate rocks, an increase in porosity was observed. After 100 years of sequestration, the porosity of the carbonate rocks and shale caprock increased by 0.16% and 0.89% respectively, for the CO_2-only case; and slightly increased by 0.17% and 0.91% respectively, for the CO_2-H_2S co-injection case. However, in the case of CO_2-SO_2 co-injection, the porosity of the carbonate rocks decreased by 0.58%, while the porosity of the shale caprock increased by 1.21%.

Table 19: Change in petrophysical properties of the formation at different times of CO_2 geosequestration at temperature and pressure of 40^0C and 100 bar, respectively.

Formation type	**Petrophysics**	**After sequestration, t=100 years**		
		CO_2	**CO_2-H_2S**	**CO_2-SO_2**
Shale	Change in porosity (%)	0.63 - 0.89	0.63 - 0.91	0.63 - 1.21
	Change in permeability (%)	1.97 - 2.81	2.01 - 2.93	2.01 - 3.86
Impure limestone	Change in porosity (%)	0.10 - 0.11	0.11 - 0.12	-ve (0.48 - 0.58)
	Change in permeability (%)	0.36 - 0.39	0.36 - 0.40	-ve (1.67 - 2.01)
Pure limestone	Change in porosity (%)	0.12 - 0.16	0.12 - 0.17	-ve (0.35 - 0.50)
	Change in permeability (%)	0.48 - 0.66	0.49 - 0.69	-ve (1.42 – 2.00)

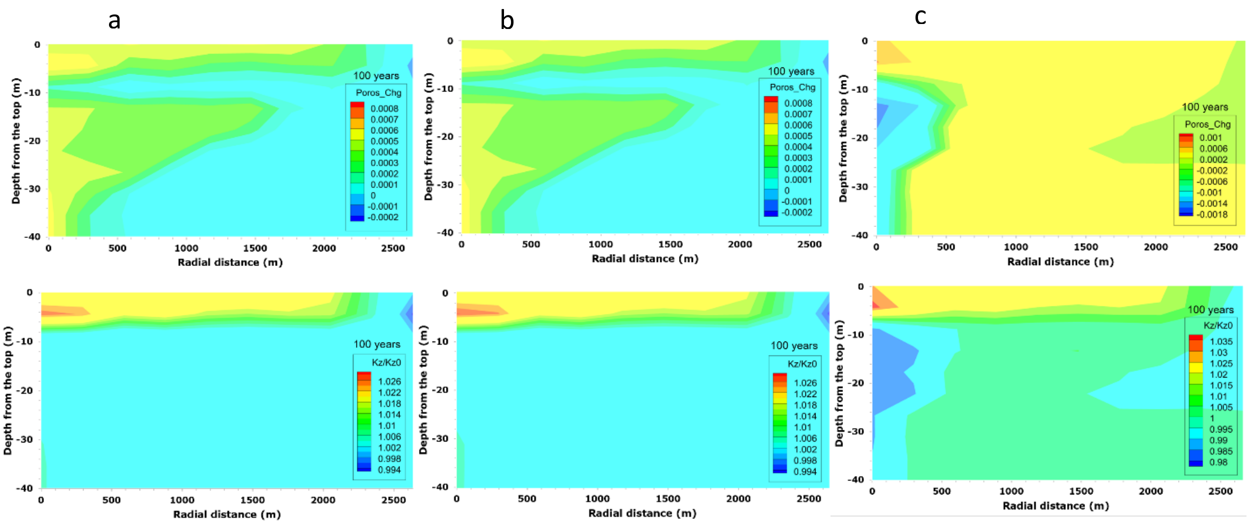

Figure 13: Porosity change and permeability ratio (a) CO_2 alone (b) CO_2-H_2S (c) CO_2-SO_2 cases at 40^0C and 100 bar.

A similar trend in porosity was observed in the CO_2 sequestration cases at higher formation salinity and temperature. The only difference is that the porosity of the shale caprock decreased during CO_2 sequestration as shown in Table 20 and Figure 14. Even though calcite precipitated in the impure limestone in the CO_2-only case at high temperature and pressure conditions (and high formation salinity), porosity increased, since very little amount of calcite precipitated (dominated by dissolution of other minerals). So, at higher temperature (100^0C) and salinity (0.21), the porosity of the carbonate rocks increased by 0.06%, while the porosity of the shale caprock decreased by 7.44% for the CO_2-only case. In the case of CO_2-SO_2 co-injection case, porosity decreased by 1.27% and 7.44% in the carbonate rocks and shale caprock, respectively. This implies that only CO_2 migrated to the caprock zone, SO_2 gas front did not reach the shale formation as rapid dissolution of SO_2 occurs at high temperature and pressure conditions. Kozeny-Carman model was used to calculate the corresponding changes in permeability. The trend of permeability variation is similar to that of porosity as shown in Table 20.

Table 20: Change in petrophysical properties of the formation at different times of CO_2 geosequestration at temperature and pressure of 100^0C and 137 bar, respectively.

Formation type	**Petrophysics**	**After sequestration, t=100 years**	
		CO_2	**CO_2-SO_2**
Shale	Change in porosity (%)	-ve (0.64 - 7.44)	-ve (0.64 - 7.44)
	Change in permeability (%)	-ve (2.02 - 21.58)	-ve (2.02- 21.60)
Impure limestone	Change in porosity (%)	0.008 – 0.01	-ve (0.04 – 0.33)
	Change in permeability (%)	0.03 – 0.05	-ve (0.14 – 1.21)
Pure limestone	Change in porosity (%)	0.01 – 0.06	-ve (0.63 - 1.27)
	Change in permeability (%)	0.05 – 0.22	-ve (2.33 - 4.60)

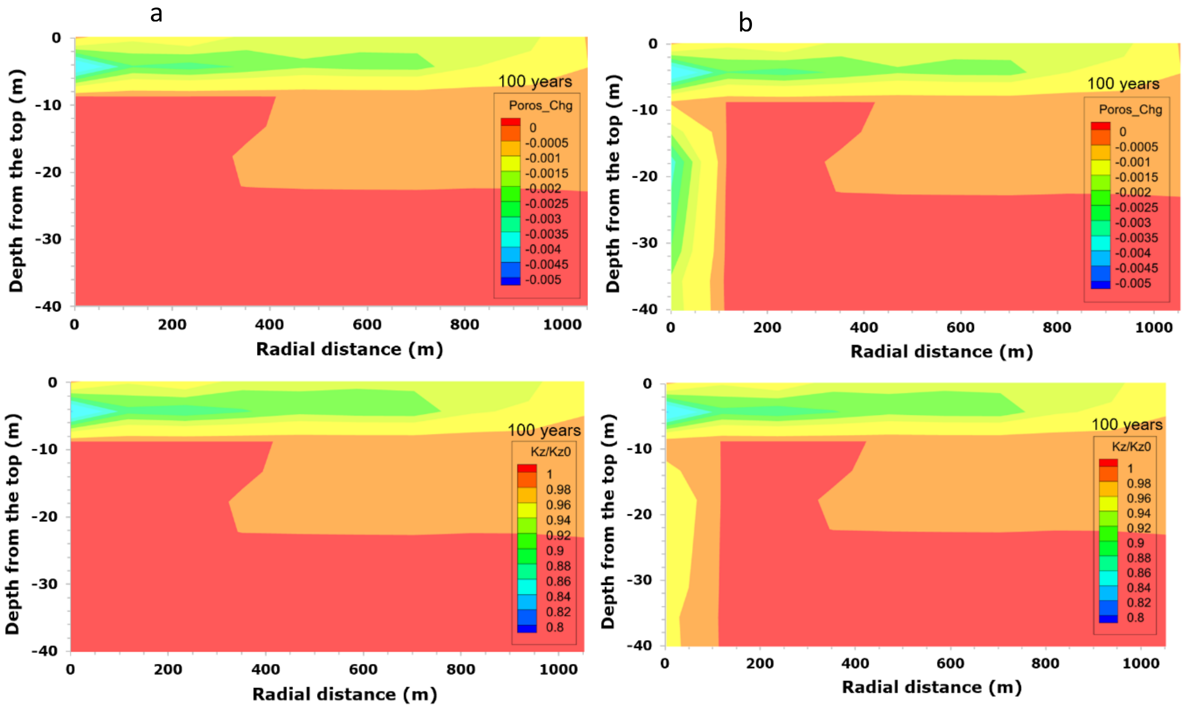

Figure 14: Porosity change and permeability ratio (a) CO_2 alone (b) CO_2-SO_2 cases at 100^0C and 137 bar.

Table 19 shows the permeability changes in the formations at 40^0C and 100 bar. After 100 years of sequestration, the permeability of the carbonate rocks and shale caprock increased by 0.66% and 2.81% respectively, for the CO_2-only case; and slightly increased by 0.69% and

2.93% respectively, for the CO_2-H_2S co-injection case. However, in the case of CO_2-SO_2 co-injection, the permeability of the carbonate rocks decreased by 2.01%, while the permeability of the shale caprock increased by 3.86%. A similar trend in permeability was observed in the CO_2 sequestration cases at higher formation salinity and temperature (Table 20). The only difference is that the permeability of the shale caprock decreased during CO_2 sequestration. Even though calcite precipitated in the impure limestone in the CO_2-only case at high temperature and pressure conditions (and high formation salinity), permeability increased, since very little amount of calcite precipitated (dominated by dissolution of other minerals). So, at a higher temperature (100^0C) and salinity (0.21), the permeability of the carbonate rocks increased by 0.22%, while the permeability of the shale caprock decreased by 21.58% for the CO_2-only case. In the case of CO_2-SO_2 co-injection case, permeability decreased by 4.60% and 21.60% in the carbonate rocks and shale caprock, respectively.

4.1.2 Impact of impurities on porosity, permeability, and geochemical composition of reservoir and cap rocks during CO_2 injection, withdrawal and storage (Strategy 2)

In strategy 2, carbonate reservoir with shale caprock and sandstone reservoir with shale caprock were considered separately. The fluid distributions and pH are similar to strategy 1 for the different formation combinations considered. In strategy 2, for all the cases considered, dissolution and precipitation of minerals in the shale formation are similar. Calcite, anhydrite, albite, chlorite, illite, k-feldspar, and kaolinite dissolved in the shale formation; while ankerite, quartz, siderite, smectite-Ca, smectite-Na, and little amount of pyrite precipitated. In the sandstone formation, dissolution of calcite, albite, chlorite, k-feldspar, and kaolinite was observed; while illite, quartz, smectite-Ca, and smectite-Na precipitated. In addition, pyrite precipitated in the CO_2-H_2S and CO_2-SO_2 co-injection cases; while anhydrite precipitated only in the CO_2-SO_2 co-injection case. In the carbonate formation, initially composed of calcite and dolomite minerals only, dissolution of dolomite was observed in all the injection cases. Calcite dissolution was observed near the injection zone for the CO_2-SO_2 case, where the concentration of dissolved SO_2 is higher, resulting in precipitation of anhydrite in that zone; while calcite precipitation was observed in the upper part of the reservoir (few metres above the injection zone). The dissolution of dolomite (increasing Mg^{2+} and Ca^{2+} concentration in the carbonate formation) resulted in precipitation of magnesite and calcite in the formation. Pyrite precipitation was only observed in the CO_2-H_2S and CO_2-SO_2 co-injection cases, although little amount as the Fe^{2+} concentration in the carbonate formation is low.

Changes in porosity of the formations are calculated from variations in the volume fraction of the minerals. Table 21 shows that porosity and permeability increased slightly in the shale formation (less than 0.5% increase in permeability), but increased significantly in the carbonate formation (due to large amount of dolomite dissolution) for all the cases considered in strategy 2 (permeability increase between 0.59 – 5.68%). In the sandstone formation, porosity and permeability only increased for the CO_2 only and CO_2-H_2S injection cases (permeability increase between 0.23 – 1.09%). Precipitation of anhydrite (few metres from the injection well over the entire height of the sandstone formation) for the CO_2-SO_2 co-injection case resulted in decrease in porosity and permeability in the region where SO_2 dissolved in formation water (permeability decrease up to 2.40%). Farther away from the injection well, porosity and permeability of the reservoir increased as more CO_2 dissolved in the formation water (very little or no concentration of SO_2 in the formation water in that region).

Table 21: Change in petrophysical properties of the formation after 100 years of CO_2 geosequestration at temperature and pressure of 40^0C and 100 bar, respectively (strategy 2).

Formation type	**Petrophysics**	**After sequestration, t=100 years**		
		CO_2	**CO_2-H_2S**	**CO_2-SO_2**
Shale	Change in porosity (%)	0.00 - 0.13	0.00 – 0.16	0.00 – 0.11
	Change in permeability (%)	0.00 - 0.39	0.00 – 0.47	0.00 – 0.34
Sandstone	Change in porosity (%)	0.07 – 0.27	0.06 – 0.25	-ve (0.29 - 0.61)
	Change in permeability (%)	0.28 – 1.09	0.23 – 1.02	-ve (1.18 - 2.40)
Carbonate	Change in porosity (%)	0.21 – 0.76	0.15 – 1.00	0.08 – 1.38
	Change in permeability (%)	0.84 -3.11	0.59 – 4.10	0.32 – 5.68

4.1.3 Impact of impurities on brittleness of reservoir and cap rocks during CO_2 geosequestration (Strategy 1)

The brittleness of rocks can be evaluated by their brittleness index. In this study, the mechanical brittleness of rock is determined using the ratio of unconfined compressive strength to the Brazilian tensile strength (BI_2), the ratio of the difference to the sum of the unconfined compressive strength and the Brazilian tensile strength (BI_3), and the ratio of static Young's modulus to static Poisson's ratio of the rock (BI_4). On the other hand, the mineralogical brittleness index can be evaluated using the ratio of the sum of the weight of brittle minerals (calcite, dolomite, feldspar, quartz, and pyrite) to the total weight of minerals in the [solid] rock (BI_{min}). In addition, the mineralogical brittleness index can be evaluated, taking into consideration the bulk modulus of the minerals and their relative level of brittleness (BI_{bm}). Thus, these two models of mineralogical brittleness were derived in this study using the volume fraction, molecular weight, and molar volume of minerals in the [solid] rock. However, a simplifying assumption of equal molar volume of minerals was made in the analysis, as the majority of the minerals considered in this study have a similar surface area, except some clay minerals such as smectite-Ca, smectite-Na, illite, and kaolinite which have relatively larger mineral surface areas and possibly higher molar volumes.

The mechanical brittleness index of the pure limestone formation before and after CO_2 geosequestration, evaluated at temperature and pressure condition of 100^0C and 137 bar (~ 2000 psi), respectively, is presented in Table 22. The increase in brittleness index of the rock using BI_2, BI_3, and BI_4 is 1.73%, 0.24%, and 31.09%, respectively.

Table 22: Mechanical brittleness index of pure limestone evaluated at 100^0C and 137 bar.

Mechanical brittleness index	**Before CO_2 sequestration**	**After CO_2 sequestration (90 days)**	**Increase in brittleness index (%)**
$BI_2 = \frac{\sigma_c}{\sigma_t}$	12.38	12.594	1.73
$BI_3 = \frac{\sigma_c - \sigma_t}{\sigma_c + \sigma_t}$	0.851	0.853	0.24
$BI_4 = E/v$	45.8357	60.0858	31.09

The mineralogical brittleness index of the pure limestone using volume fraction of minerals obtained from numerical simulations of the experimental condition and molecular weight of the minerals, BI_{bm} and BI_{min} remained constant as 0.51 and 1.00, respectively after 90 days of CO_2 sequestration. This is because no mineral precipitated in the pure limestone formation after 90 days of CO_2 sequestration; calcite dissolution continues. In fact, the simulation was run further for 100 years, yet no mineral precipitated. So, the mineralogical brittleness index of the pure limestone remained constant. The mineralogical brittleness index of the rock correlates with the mechanical brittleness index (BI_3), as there is no significant increase in the brittleness of the pure limestone before and after CO_2 geosequestration. Therefore, BI_2 and BI_4 models of estimating the mechanical brittleness index of pure limestone exaggerate their brittleness. The mechanical brittleness index of the pure limestone, evaluated using the ratio of the difference to the sum of the unconfined compressive strength and the Brazilian tensile strength of the rock (BI_3), is more accurate.

The mineralogical brittleness index of the carbonate rocks and shale caprock was evaluated at the same temperature and pressure condition (100^{0}C and 137 bar) for the co-injection cases, to evaluate the impact of impurities in CO_2 on the brittleness of rocks (Table 23).

Table 23: Brittleness index of the formation at different times of CO_2 geosequestration at temperature and pressure of 100^{0}C and 137 bar, respectively.

Formation type	**Brittleness index**	**Before sequestration, t=0**			**During sequestration, t=90 days**			**After sequestration, t=100 years**		
		CO_2	**CO_2-H_2S**	**CO_2-SO_2**	**CO_2**	**CO_2-H_2S**	**CO_2-SO_2**	**CO_2**	**CO_2-H_2S**	**CO_2-SO_2**
Shale	BI_{bm}	0.0490	0.0490	0.0490	0.0490	0.0489 – 0.0490	0.0489 – 0.0490	0.0377-0.0420	-	0.0377-0.0419
	BI_{min}	0.0898	0.0898	0.0898	0.0895 - 0.0896	0.0895	0.0895	0.0634 -0.0721	-	0.0635-0.0721
	BI_{mech}	-	-	-	-	-		-	-	
Impure limestone	BI_{bm}	0.5091	0.5091	0.5091	0.5091	0.5091	0.5047-0.5084	0.5090	-	0.5045-0.5087
	BI_{min}	0.9984	0.9984	0.9984	0.9984	0.9984	0.9896-0.9968	0.9980	-	0.9895 - 0.9966
	BI_{mech}	-	-	-	-	-		-	-	-
Pure limestone	BI_{bm}	0.5100	0.5100	0.5100	0.5100	0.5100	0.4941-0.5027	0.5100	-	0.4938-0.5024
	BI_{min}	1.0000	1.0000	1.0000	1.0000	1.0000	0.9692 – 0.9858	1.0000	-	0.9679-0.9851
	BI_{mech}	0.850	0.850	0.850	0.853	-	-	-	-	-

The result showed that the brittleness of the carbonate rocks remained relatively constant after 90 days of sequestration for the CO_2 alone case, while the brittleness of the carbonate rocks decreased for the CO_2-SO_2 co-injection case. The brittleness of the shale formation decreased for all the injection cases. However, the reduction in brittleness of the shale caprock was only due to the upward migration of CO_2 by buoyant forces. SO_2 did not migrate to the shale caprock, due to preferential dissolution of SO_2 gas in the carbonate formation water. Even after 100 years, SO_2 never migrated to the shale formation (Figure 15).

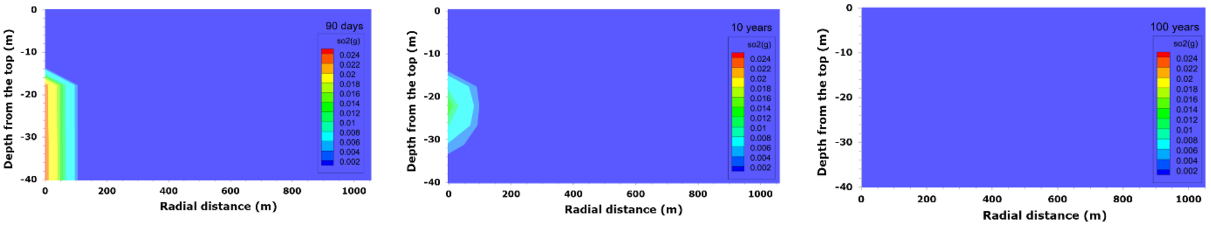

Figure 15: SO_2 gas in the formations at 100^{0}C and 137 bar (salinity=0.21) after 90 days, 10 years, and 100 years of CO_2 sequestration.

It is worth noting that under this condition (100^{0}C and 137 bar), CO_2 was injected for 90 days only and the sequestration period was 100 years. So, it is possible that SO_2 could have reached the shale caprock if the gas injection period was up to 10 years, which is a realistic CO_2 injection period. Therefore, further numerical simulations were performed to evaluate the brittleness of rocks in low-temperature formations.

The brittleness of carbonate and shale formations was evaluated at temperature and pressure conditions of 40^{0}C and 100 bar, respectively. The CO_2 gas (with or without impurities) was injected for 10 years. SO_2 (or H_2S) gas reached the shale caprock during the sequestration period for the co-injection cases. The brittleness index of the rocks at different times of the sequestration are shown in Table 24. There is no significant increase or decrease in the brittleness of carbonate and shale rocks for the CO_2 alone and CO_2-H_2S co-injection cases. Furthermore, for the CO_2-SO_2 co-injection case, there is no significant decrease in the brittleness of shale caprock. However, the brittleness of the carbonate rocks decreased significantly in the CO_2-SO_2 co-injection case. The decrease in brittleness in the carbonate rocks is due to precipitation of anhydrite. Anhydrite did not precipitate in the shale caprock, hence the slight decrease in brittleness of the shale formation is similar in all the cases considered. A very little amount of pyrite precipitation was observed in the CO_2-H_2S and CO_2-SO_2 co-injection cases. Therefore, pyrite precipitation did not significantly impact brittleness of the rocks.

Table 24: Brittleness index of the formation at different times of CO_2 geosequestration at temperature and pressure of 40^{0}C and 100 bar, respectively (strategy 1).

Formation type	**Brittleness index**	**Before sequestration, t=0**			**During sequestration, t=90 days**			**After sequestration, t=100 years**		
		CO_2	**CO_2-H_2S**	**CO_2-SO_2**	**CO_2**	**CO_2-H_2S**	**CO_2-SO_2**	**CO_2**	**CO_2-H_2S**	**CO_2-SO_2**
Shale	BI_{bm}	0.0490	0.0490	0.0490	0.0489-0.4900	0.0489-0.0490	0.0489-0.0490	0.0486-0.0487	0.0487	0.0487-0.0488
	BI_{min}	0.0898	0.0898	0.0898	0.0895-0.0898	0.0895-0.0898	0.0895-0.0898	0.0888-0.0889	0.0888-0.0890	0.0890-0.0891
Impure limestone	BI_{bm}	0.5091	0.5091	0.5091	0.5091	0.5091	0.5091	0.5092	0.5091-0.5092	0.5026-0.5043
	BI_{min}	0.9984	0.9984	0.9984	0.9984	0.9984	0.9983-0.9984	0.9984	0.9984	0.9856-0.9889
Pure limestone	BI_{bm}	0.5100	0.5100	0.5100	0.5100	0.5100	0.4979-0.5076	0.5100	0.5100	0.4979-0.4996
	BI_{min}	1.0000	1.0000	1.0000	1.0000	1.0000	0.9768-0.9953	1.0000	1.0000	0.9763-0.9797

Overall, the brittleness of the shale caprock decreased slightly during CO_2 geosequestration (with or without impurities), while the brittleness of carbonate rocks is relatively constant for CO_2

alone and CO_2-H_2S co-injection cases. However, the brittleness of carbonate rocks decreased significantly for the CO_2-SO_2 co-injection case. These results imply that shale formations are preferable for cap rocks, as their brittleness decreases during CO_2 geosequestration. Carbonate formations can also be suitable as cap rocks during co-injection of CO_2 with SO_2 gas in depleted petroleum reservoirs or aquifers, as the brittleness of the carbonate rocks decreases in this case. During CO_2 geosequestration (with or without H_2S), carbonate formations are suitable reservoir rocks as their brittleness is relatively constant (easier to fracture when needed, for enhanced fluid recovery or production activity), and CO_2 injection and storage capacity of the carbonate reservoirs are maintained as the porosity and permeability of the formation remains constant or increases slightly.

4.1.4 Impact of impurities on brittleness of reservoir and cap rocks during CO_2 geosequestration (Strategy 2)

The brittleness of carbonate, sandstone, and shale formations was evaluated at temperature and pressure conditions of 40^0C and 100 bar, respectively. Table 25 shows that the brittleness of the sandstone (0.4593) is higher than that of the carbonate formation (0.4586) before CO_2 sequestration; while the brittleness of the shale formation is relatively very low (0.0377). The relatively higher brittleness of sandstone formation before CO_2 sequestration is due to the high amount of the initial quartz and feldspar minerals, and some amount of calcite. The CO_2 gas (with or without impurities) was injected for 10 years. SO_2 (or H_2S) gas hardly contacted the shale caprock (very low mole fraction, as higher concentration of SO_2 or H_2S is in the reservoir due to preferential dissolution of SO_2 (or H_2S) gas in the formation water. Thus, the brittleness of the shale caprock is largely dependent on the reaction of CO_2 with the rock minerals. Hence, the brittleness of the shale caprock for all the injection cases are similar and decreased slightly during the period of CO_2 geosequestration.

Table 25: Brittleness index of the formation before and after CO_2 geosequestration at temperature and pressure of 40^0C and 100 bar, respectively (strategy 2).

Formation type	**Brittleness index**	**Before sequestration, t=0**			**After sequestration, t=100 years**		
		CO_2	**CO_2-H_2S**	**CO_2-SO_2**	**CO_2**	**CO_2-H_2S**	**CO_2-SO_2**
Shale	BI_{bm}	0.0377	0.0377	0.0377	0.0375 – 0.0376	0.0375 – 0.0376	0.0374 – 0.0376
Sandstone	BI_{bm}	0.4593	0.4593	0.4593	0.4591 – 0.4592	0.4591 – 0.4592	0.4533 – 0.4551
Carbonate	BI_{bm}	0.4586	0.4586	0.4586	0.4587 – 0.4591	0.4587 – 0.4592	0.4548 – 0.4592

Meanwhile, the brittleness of the sandstone formation decreased (slightly for the CO_2 only and CO_2-H_2S injection cases, and significantly for the CO_2-SO_2 co-injection case) for all the injection cases, due to dissolution of most of the brittle minerals (calcite, albite, and k-feldspar) and precipitation of more non-brittle and clay minerals such as illite, smectite-Ca, smectite-Na, and anhydrite (for the CO_2-SO_2 co-injection case). However, the brittleness of the carbonate reservoir increased for the CO_2 only and CO_2-H_2S injection cases as more dolomite dissolves and triggering calcite precipitation. Considering the relative brittleness of different brittle minerals, the coefficient of the weight fraction of calcite is higher than that of dolomite (coefficient applied in the developed mineralogical brittleness index model in the present study, to account for the relative brittleness of the minerals) and the amount of magnesite that precipitated is too low (its effect on the brittleness index is negligible), resulting in increased brittleness of the carbonate formation during CO_2 geosequestration (with or without H_2S). Surprisingly, for the CO_2-SO_2 co-injection case, brittleness increased in the upper part of the carbonate reservoir and decreased in its lower part. This is because calcite precipitated in the upper part of the reservoir (no anhydrite), while anhydrite precipitated in the lower part of the carbonate reservoir in the region where the concentration of dissolved SO_2 is high (as calcite and dolomite dissolved). Therefore, in the regions with very little or no dissolved SO_2 in formation water, brittleness of the carbonate reservoir increases.

The mathematical model developed in the present study can be extended to CO_2 co-injection cases with contaminants (impurities). The model is validated with an existing model (Kang et al., 2020) that utilizes weight fraction of minerals, to evaluate brittleness index using the experimental results published by Mavhengere et al. (2022). The estimated brittleness index based on the model developed by Kang et al. (2020) is shown in Table 26. Both the existing model developed and the model developed in the present study (based on the molecular weight and volume fraction of minerals) account for the significant change in the brittleness of reservoir or sandstone rocks when SO_2 is co-injected with CO_2. With pure CO_2, the change in the brittleness index of both ZC and ZG is negligible, but changes significantly with CO_2-SO_2 mixture.

Table 26: Brittleness index of ZC and ZG based on the weight fraction of their minerals and considering the relative level of brittleness of each brittle mineral based on bulk modulus

Sample	**Quartz (wt. %)**	**Plagioclase (wt. %)**	**Smectite (wt. %)**	**Calcite (wt. %)**	**Pyrite (wt. %)**	**Stilbite (wt. %)**	**Diopside (wt. %)**	**Gypsum (wt. %)**	**Orthoclase (wt. %)**	**BI_{bm}**
ZC untreacted	44.1	44.7	1.0	3.5	0.4	3.6	2.7	0.0	0.0	0.68
ZC CO_2 treated	47.5	42.5	2.5	1.7	0.4	2.7	2.8	0.0	0.0	0.69
ZC CO_2-SO_2 treated	49.1	28.6	11.8	0.0	0.8	4.9	2.3	2.5	0.0	0.63
ZG untreacted	21.5	46.0	22.2	0.0	0.0	2.0	0.0	0.0	8.3	0.52
ZG CO_2 treated	22.3	50.5	16.3	2.9	0.0	4.8	0.0	0.0	3.2	0.52
ZG CO_2-SO_2 treated	26.1	53.4	12.1	2.3	0.0	0.0	0.0	0.0	6.2	0.60

The alteration in the mineral phases of the ZC rock sample is similar to the sandstone reservoir in the present study, as CO_2-SO_2 mixture resulted in decrease in brittleness index of the rock; therefore, ZC sandstone was used to validate the mathematical model in the present study. Unlike ZC, for ZG, smectite (clay mineral) and stilbite dissolution was observed, while plagioclase and calcite precipitated, thereby inhibiting the precipitation of gypsum and increased brittleness index in the CO_2-SO_2 mixture case. The difference in the chemical reaction in the ZC and ZG sandstones is due to their mineralogical composition. For example, ZG rock sample does not have calcite, pyrite and diopside as primary minerals; whereas those are some of the primary minerals in ZC rock sample. Hence, only gypsum precipitated as secondary mineral in ZC rock sample, while calcite precipitated as secondary minerals in ZG rock sample. Therefore, the impact of contaminants on brittleness index of rocks depends on their (rocks') mineralogical composition. Furthermore, although the samples (sandstone samples from Zululand Basin) were held in the reactors in the CO_2 and gas mixture only for 2 months, this analysis confirms that the change in the brittleness index of rocks during the storage of pure CO_2 is negligible compared to how much CO_2-SO_2 mixture alters the brittleness of rocks.

4.2 Discussion of Key Findings

Findings of the study revealed that after injection, some mass of CO_2 gas is trapped in the reservoir rocks with higher porosity and permeability, and certain amount of CO_2 gas begins to dissolve in the formation water; while the mobile CO_2 gas continues to migrate into the shale caprock (with lower porosity and permeability) by buoyancy forces. Meanwhile, the fronts of SO_2 (or H_2S) gas is behind that of CO_2 due to preferential dissolution of these gases in formation water compared to CO_2. This finding is consistent with a numerical modeling study conducted by Zhang et al. (2010) on the fate and transport of co-injection of H_2S with CO_2 in deep saline formations. They found that the mass fraction of CO_2 at the advancing gas front was higher than that of the H_2S gas. However, they did not consider SO_2 gas and the migration of injected gas to the low-permeability caprock. Findings of the present study showed that SO_2 gas front is far behind that of H_2S and CO_2 gas fronts, and the mole fractions of the impurities (for the co-injection cases) in CO_2 decrease as the injected gas migrates vertically and horizontally in the formations up to the caprock zone. In fact, at higher temperature and pressure (and salinity up to 0.21) conditions, SO_2 gas completely dissolved in the formation water after 100 years of sequestration (when injection period was only 90 days). In addition, the concentration of total dissolved carbon in the co-injection cases is lower than that in the CO_2 alone case, which is also in line with the findings of Zhang et al. (2010). In the CO_2-SO_2 co-injection case, after 100 years of sequestration, the TDC near the injection well (up to 25 m radial distance) is relatively low compared to the CO_2 alone and CO_2-H_2S co-injection cases. This is due to rapid dissolution of SO_2 gas in formation water. Thus, as soon as SO_2 comes into contact with formation water during injection, it begins to dissolve near the injection well and go into aqueous phase, inhibiting the dissolution of CO_2 gas in that region. Therefore, H_2S gas is able to migrate more laterally and vertically with the CO_2 gas, as H_2S gas dissolution is less rapid relative to SO_2 gas.

Furthermore, dissolution of chlorite, albite, dolomite, and k-feldspar was observed in the shale and impure limestone formations; while quartz, illite, smectite-Ca, and smectite-Na precipitated in those formations (strategy 1). The mineral reactions are consistent with the findings in the study conducted (up to 5000 years of sequestration) by Ma et al. (2019). However, in strategy 1, calcite did not dissolve in the shale caprock during the sequestration period (0-100 years). But calcite, anhydrite, and illiite dissolved (in the shale caprock) in strategy 2 of the simulation, to provide enough Ca^{2+} and Mg^{2+} for ankerite precipitation as no dolomite mineral was initially in the shale caprock (strategy 2). At higher temperature (100^0C) and salinity ($X_s = 0.21$), calcite precipitated in the shale and impure limestone formations (strategy 1) during CO_2 alone injection case. The precipitation of calcite in the impure limestone formation attenuated the Ca^{2+} concentration, triggering rapid dissolution of dolomite and precipitation of clay minerals (especially, illite and smectite-Na). Thus, this finding revealed that the percentage of brittle minerals in the impure limestone formation decreased slightly during CO_2 alone sequestration at 100^0C and salinity of 0.21.

Findings of the study revealed that in the CO_2-H_2S co-injection case (strategy 1), no ankerite and siderite precipitation in the carbonate rocks. Only little amount of ankerite was observed in the shale caprock in the region where dissolved H_2S in the formation water is low in concentration. But, significant amount of ankerite precipitated in the shale caprock in strategy 2 of the simulations, due to adequate amount of Ca^{2+} and Mg^{2+} from calcite, anhydrite and illite dissolution. Pyrite precipitation was observed in all the formations considered, in the regions where H_2S dissolved in the formation water. This result is in line with the findings of Zhang et al. (2010), and can be attributed to the fact that precipitation of ankerite and siderite requires Fe^{2+} which can be supplied by the dissolution of iron-bearing minerals such as chlorite. Thus, as CO_2 is co-injected with H_2S, pyrite precipitates (using up most of the Fe^{2+} concentration as H_2S preferentially dissolves in the formation water, delaying CO_2 gas dissolution), inhibiting the precipitation of ankerite and siderite. Furthermore, in the CO_2-SO_2 co-injection case, after 100 years of sequestration, ankerite, magnesite, and pyrite precipitated in the shale caprock; while anhydrite and pyrite mainly precipitated in the carbonate rocks, in the region where SO_2 gas dissolved in formation water. Meanwhile, outside this region, ankerite, siderite, and magnesite precipitation were observed in the shale and impure limestone formations. Therefore, CO_2-SO_2 co-injection, creates a better environment for ankerite and siderite precipitation in the formations. Moreover, in the CO_2 alone case, ankerite precipitation was observed in the shale caprock and impure limestone (from the injection well) formations as precipitation and dissolution of pyrite was negligible (without CO_2 co-injection with SO_2 or H_2S). But no ankerite precipitation (mainly pyrite precipitation) in the carbonate and sandstone formations in strategy 2 of the simulation. This confirms that precipitation of pyrite inhibits ankerite precipitation during CO_2 co-injection with H_2S or SO_2 (Zhang et al. 2010).

During the 100 years of CO_2 geosequestration, minerals such as quartz and smectite-Na precipitated in some layers of the pure limestone formation. This is due to the fluid interaction between different formations in the CO_2 gas storage field. A ‘fingering’ flow pattern exists near the bottom of the CO_2 plume as density of the aqueous-phase increases due to CO_2 dissolution (Xu et al., 2011). Thus, there is advection in the aqueous-phase, enabling fluids in one formation (vertically above) to mix with fluids in another formation (relatively, vertically below). Therefore, fluids in the shale caprock contact fluids in the impure limestone, and fluids in the impure limestone contact fluids in the pure limestone formation during the CO_2 geosequestration. Hence, the petrophysical and geochemical properties of the formations are altered by the fluid-rock interactions, such that these formations exhibit unusual characteristics that could not have been possible if the formations or layers were vertically homogeneous.

Findings of the study revealed that in strategy 1, porosity and permeability increase in the shale and carbonate rocks, in the CO_2 alone and CO_2-H_2S co-injections cases; while in the CO_2-SO_2 co-injection case, porosity and permeability increase only in the shale rock, and decrease in the carbonate rocks due to anhydrite precipitation. However, beyond the regions where SO_2 dissolved in the formation water in the carbonate rocks, increase in porosity and permeability was observed. Meanwhile, in strategy 2 of the simulation, porosity and permeability increase in the carbonate formation for all the injection cases; while porosity and permeability increase in the sandstone reservoir for the CO_2 only and CO_2-H_2S injection cases, but decreased for the CO_2-SO_2 injection case (in the regions where SO_2 dissolved in the formation water). In strategy 2, the increase in porosity and permeability of the carbonate rock for the CO_2-SO_2 injection case is due to the severe dolomite dissolution compared to anhydrite and pyrite precipitation. These findings are consistent with the results of some scholars (Alam et al., 2014, Bolourinejad and Herber, 2014; Pearce et al., 2016; Aminu et al., 2018). However, in the studies conducted by Bolourinejad and Herber (2014) and Aminu et al. (2018), porosity and permeability decreased in the reservoir during CO_2-H_2S co-injection. This result is different in the present study, as only little amount of pyrite precipitated due to low concentration of Fe^{2+} in the formation. Thus, the porosity and permeability of the carbonate rocks increased instead.

Furthermore, the porosity and permeability of the shale caprock decreased during CO_2 geosequestration (with or without SO_2) at higher temperature (100^{0}C) and salinity (0.21). This finding is in agreement with the results of Ma et al. (2019), as increase in salinity results in increase in the concentration of ions in the caprock and reduce the dissolution effect of the shale caprock. Ma et al. (2019) found that at a lower salinity, an increase in temperature from 47^{0}C to 57^{0}C enhanced dissolution of the caprock (in 5000 years), and mineral dissolution-domination in the mineralization reaction further increases the permeability of the caprock. Therefore, the decrease in porosity and permeability in the present study, when temperature and salinity were up to 100^{0}C and 0.21, respectively, was mainly impacted by the high salinity of the formation. However, temperature might have had some level of impact on the decrease in the porosity and permeability of the rock (even though not as much as the impact of the formation salinity), as Davila et al. (2017) found that porosity of crushed marl caprock increased more at lower temperature, while porosity reduced as temperature increased.

The fluid-rock interactions during CO_2 geosequestration, impact the mineral composition of the rocks and alter their brittleness. In the present study, the mechanical brittleness index (determined based on ratio of the difference to the sum of unconfined compressive strength and Brazilian tensile strength of the rock) of the pure limestone and the mineralogical brittleness index correlates. As expected, the mineralogical brittleness index and the mechanical brittleness index of the pure limestone formation remained constant during CO_2 alone sequestration (no significant difference in the brittleness index before and after CO_2 sequestration) at 100^{0}C and 137 bar (and salinity up to 0.21). This is because no mineral precipitated in the pure limestone formation during the period of geosequestration (0 - 100 years). Therefore, mechanical brittleness index of rocks evaluated using the simple ratio of unconfined compressive strength to tensile strength and the ratio of Young's modulus to Poisson's ratio exaggerates brittleness or ductility of the rocks. Meng et al. (2015) and Zhang et al. (2016) confirm the failure of these approaches of evaluating mechanical brittleness index of rocks, as the evaluation of brittleness index of rocks based on [simple] strength ratio or product or ratio of elastic modulus to Poisson's ratio cannot properly describe their brittleness. They believe that the brittleness of rocks depends on other factors including bulk modulus, pore pressure, and stress-state of the rock. Thus, in the present study, the mechanical brittleness index determined based on ratio of the difference to the sum of unconfined compressive strength and Brazilian tensile strength of the rock is more accurate. The accuracy of this approach of evaluating mechanical brittleness index, validates the mineralogical brittleness index models developed in this study. Therefore, the mineralogical brittleness index models are extended to evaluate the impact of impurities on the brittleness of shale and carbonate rocks during CO_2 geosequestration. After 100 years of sequestration (in the CO_2 alone case), the brittleness of the impure limestone formation decreased slightly as more clay minerals precipitated (since calcite precipitation, in the impure limestone at 100^0C temperature and 0.21 salinity, triggered rapid dissolution of dolomite). Under the same conditions of sequestration (100^0C and 137 bar), the brittleness of the carbonate rocks (pure and impure limestone) decreased for the CO_2-SO_2 co-injection case.

Meanwhile, the brittleness of the shale formation decreased for all the injection cases at 100^0C and 137 bar (and salinity of 0.21). However, the reduction in brittleness of the shale caprock was mainly due to the upward migration of CO_2 by buoyant forces and precipitation of more clay minerals, as SO_2 did not migrate to the shale caprock, due to the preferential dissolution of SO_2 gas in the carbonate formation water. Moreover, during CO_2 geosequestration condition of 40^0C and 100 bar, CO_2 gas reached the shale caprock and some amount of SO_2 (or H_2S) gas, as the initial petrophysical properties of the formations were increased slightly during the numerical simulation. In strategy 1 of the simulations, the brittleness of the shale caprock decreased slightly during CO_2 geosequestration (with or without SO_2/H_2S impurities), while the brittleness of the carbonate rocks remain relatively constant for CO_2 alone and CO_2-H_2S co-injection cases. However, the brittleness of the carbonate rocks decreased significantly for the CO_2-SO_2 co-injection case. Meanwhile, in strategy 2 of the simulations, brittleness of the shale caprock and sandstone reservoir decreased slightly during the period of CO_2 geosequestration for all the injection cases; while brittleness of the carbonate reservoir increased for the CO_2 only and CO_2-H_2S injection cases, but varies (decreased or increased) vertically (at the same radial distance) for the CO_2-SO_2 injection case. In the CO_2-SO_2 injection case, the upper part of the reservoir is more brittle compared to the lower part of the same carbonate reservoir (strategy 2). This is because the injected CO_2 (with or without SO_2/H_2S) in shale and sandstone formations result in dissolution of key brittle minerals and precipitation of more non-brittle and clay minerals, while the brittleness of the carbonate rocks is influenced mainly by calcite precipitation (or dissolution). Significant calcite dissolution in the presence of other minerals, corresponds decreased brittleness; while notable calcite precipitation corresponds to increased brittleness of the carbonate rock in the present study. The simple sum of weight of brittle minerals to the total weight of minerals is not accurate in carbonate formations (initially composed on brittle minerals only); thus, the mineralogical brittleness index based on the relative brittleness of the minerals is more accurate, to account for the increase or decrease in the brittleness index of the carbonate, sandstone, and shale formations.

The decrease in brittleness of the shale caprock is consistent with the results of Lyu et al. (2018). Lyu et al. (2018) adopted the energy-balance method together with the Weibull distribution-based constitutive model to calculate the brittleness values of shale rock samples with or without [CO_2-brine] soaking conditions. They found that the intact shale sample (without soaking with CO_2-brine) has the highest brittleness index value (more brittle), which is in accordance with the high percentage of brittle minerals of the shale sample. They also found that CO_2-brine-shale rock interactions decrease the brittleness values of the shale rock as well as its peak axial strength and Young's modulus. In addition, Lyu et al. (2018) found that CO_2-NaCl-shale interaction has more effect on strength and Young's modulus than brittleness of the shale rock, as the low-clay shale still keeps good fracture performance after CO_2 sequestration. CO_2-brine-rock interactions decrease the unconfined compressive strength and Brazilian tensile strength of carbonate, shale, and sandstone formations (AL-Ameri et al., 2014; Lyu et al., 2018; Heidari et al., 2020). So, even though the strength of the rocks decrease during CO_2 geosequestration, the relative change in their unconfined compressive strength and Brazilian tensile strength determines their brittleness and potential to withstand tensile fracturing. According to Gong and Zhao (2007), a rock mass with low [Brazilian] tensile strength is easily subjected to tensile fracture, and a high unconfined compressive strength assists in resisting the closure of natural and induced fractures. Therefore, it is imperative that while the strengths of the caprock decreases during CO_2 geosequestration, the relative decrease in the tensile strength is less than that of the compressive strength, to decrease brittleness of the rock and increase its potential to withstand tensile fracturing. Furthermore, ductility of caprock would allow it to deform without developing high permeability pathways that can enable CO_2 leakage

(Espinoza and Santamarina, 2017). So, instead of developing a higher permeability, the permeability decreases to reduce the chance of CO_2 leakage to the earth surface. Thus, the shale caprock at high formation temperature and pressure (and high salinity) conditions may be preferable as porosity and permeability decreases during CO_2 geosequestration as well as its brittleness.

Findings of the study suggest that shale formations are preferable for cap rocks, as they have low brittleness index and their brittleness decrease during CO_2 geosequestration for all injection cases and formation conditions. Carbonate formations are not suitable cap rocks during CO_2 geosequestration, as they are very brittle and their brittleness increases or decreases depending on the formation temperature, pressure, salinity, and impurities co-injected with supercritical CO_2. However, carbonate rocks composed of more than one carbonate mineral (for instance, calcite and dolomite) may be suitable reservoir rocks for cyclic injection of CO_2 (with or without SO_2/H_2S), as their porosity and permeability increase during CO_2 geosequestration (enabling injectivity) and carbonate formation become more brittle in the CO_2 production or withdrawal zone (enabling productivity). During the cyclic injection and withdrawal process, CO_2 stored would be mainly by residual and solubility trapping, as mineral trapping of CO_2 is not effective in carbonate formations (Zhang et al., 2010). Sandstone formation will be suitable for long-term storage of CO_2 as the change in porosity and permeability during injection is minimal, but may increase or decrease significantly after several years of storage. In addition, the change (or decrease) in brittleness is negligible; thus, the injected CO_2 would have negligible impact on the flow pathways (in terms of creating more paths to enhance fluid flow). Also, sandstone formations are more favourable for CO_2 mineral trapping than carbonate formations (Zhang et al., 2010). Thus, CO_2 can be stored (long-term) in the sandstone formation by mineral, solubility, and residual trapping mechanisms. Overall, based on the mineralogical compositions of the formations in this study, shale formations are suitable cap rocks for short- and long-term storage of CO_2; carbonate rocks (initially comprised of carbonate minerals) may be suitable reservoirs for cyclic injection of CO_2, while sandstone formations are suitable reservoirs for long-term storage of CO_2.

5.0 Conclusions and Recommendations

5.1 Conclusions

In this study, a 2-D reactive transport model was developed for geosequestration of CO_2 in reservoir formations overlain by shale caprock. Two strategies were adopted while performing the numerical simulations (namely, strategy 1 and strategy 2). In strategy 1, the formations considered are carbonate (pure and impure limestone) and shale formations. The carbonate formations are vertically heterogeneous, such that a pure limestone formation (with calcite mineral only) is overlain by an impure limestone (majorly calcite with little amount of other minerals in the shale formation) formation. Similarly, the impure limestone formation is directly overlain by a shale caprock. In strategy 2, two separate reservoir formations (carbonate and sandstone) with shale caprock were considered. Thus, the mineralogical composition and water chemistry of the formations are different. Furthermore, mathematical models were developed for evaluating mineralogical brittleness index of the formations before and after CO_2 sequestration (with or without SO_2 or H_2S). One of the mineralogical brittleness index models take into consideration the relative level of brittleness of different brittle minerals based on their bulk modulus, while the other mineralogical brittleness index model only considers the sum of the weight fraction of the brittle minerals based on their volume fraction [in solid rock], molecular weight, and molar volume (which is assumed to be the same for all the minerals in this study). Based on the key findings in this study, the conclusions from simulations and mathematical models are summarized as follows:

1. The preferential dissolution of SO_2 or H_2S gas into formation water (compared with CO_2 gas) leads to the delayed breakthrough of SO_2 or H_2S gas, and the separation between CO_2 and SO_2/H_2S gases at the moving front. The mobility of CO_2 is higher than that of SO_2/H_2S gas. In fact, the mobility of CO_2 is by far more than that of SO_2. Thus, SO_2 gas front is far behind that of CO_2 (compared to the separation between CO_2 and H_2S). In both co-injection cases, more SO_2/H_2S contains in the interior of the gas plume (during the CO_2 co-injection period, the mole fraction of SO_2/H_2S gas diminishes gradually from the injection well or perforation interval, laterally and upward as the CO_2 gas moves). CO-injection of SO_2/H_2S reduces CO_2 solubility compared to CO_2 alone case. As the mole fraction of SO_2/H_2S in the moving gas front diminishes, CO_2 dissolution in the formation water is enhanced.
2. Co-injection of H_2S with CO_2 in the formations causes the precipitation of pyrite through the chemical interactions between the dissolved H_2S and Fe^{2+} from the dissolution of iron-bearing minerals. No ankerite and siderite precipitation in the carbonate rocks; but little amount of ankerite was observed in shale caprock. Meanwhile, in the CO_2-SO_2 co-injection case, ankerite, magnesite, and pyrite precipitated in the shale caprock; while anhydrite and pyrite mainly precipitated in the carbonate and sandstone rocks. In fact, ankerite precipitated in the impure limestone (carbonate) formation. This is because the dissolution of chlorite increases Fe^{2+} and Mg^{2+} concentrations in the formation, while the precipitation of calcite in the shale caprock triggered dolomite dissolution (increasing Mg^{2+} concentration in the formation). Thus,

enough Fe^{2+} was available for the precipitation of ankerite (enhanced by the abundant concentration of Mg^{2+}) and pyrite (SO_2 dissolution mainly favoured the precipitation of pyrite, as anhydrite did not precipitate due to calcite precipitation) in the shale caprock, while Mg^{2+} promoted the precipitation of magnesite (due to CO_2 dissolution, as the mole fraction of SO_2 diminished in the shale formation). Therefore, the precipitation of pyrite inhibits ankerite precipitation. But in formations with abundance of Mg^{2+} this inhibiting effect is negligible.

3. During CO_2 sequestration (with or without SO_2/H_2S), minerals such as quartz and smectite-Na precipitated in some layers of the pure limestone formation. This is due to the advective ('fingering' flow pattern near the bottom of the CO_2 plume) transport of the high density aqueous phase (resulting from CO_2 dissolution), enabling fluids in one formation (vertically above) to mix with fluids in another formation (relatively, vertically below). Thus, unexpected minerals precipitate in the formation.
4. For the CO_2 alone and CO_2-H_2S co-injections cases, porosity and permeability increase slightly in the shale and carbonate rocks; while in the CO_2-SO_2 co-injection case, porosity and permeability increase only in the shale rock and the carbonate rock (initially containing calcite and dolomite minerals), and decrease in other carbonate and sandstone rocks due to anhydrite precipitation. The slight increase in porosity and permeability in the CO_2-H_2S co-injection case is because very little amount of pyrite precipitated due to low concentration of Fe^{2+} in the formation. Thus, increase in the porosity and permeability of the carbonate rocks was observed instead of a decrease. However, the porosity and permeability of shale caprock decreased during CO_2 sequestration (with or without SO_2/H_2S) at higher temperature and salinity of 100^0C and 0.21, respectively. Therefore, shale caprock exhibits self-sealing ability at high salinity and temperature conditions.
5. Mechanical brittleness index of rocks evaluated using the simple ratio of unconfined compressive strength to tensile strength and the ratio of Young's modulus to Poisson's ratio exaggerate brittleness or ductility of the rocks. The mechanical brittleness index determined based on ratio of the difference to the sum of unconfined compressive strength and Brazilian tensile strength of the rock is more accurate and correlates well with the mineralogical brittleness index models. The brittleness of pure limestone formation remains the same during CO_2 geosequestration (without H_2S/SO_2 gas), while the brittleness of shale caprock decreased slightly. However, the brittleness of impure limestone (carbonate) formation decreases slightly during CO_2 geosequestration at high temperature (100^0C) and salinity (0.21). At the same condition, the brittleness of the carbonate rocks (pure and impure limestone) decrease in the CO_2-SO_2 co-injection case. At low temperature (40^0C) and

salinity (0.06), the brittleness of the limestone and sandstone rocks remain relatively constant for CO_2 alone and CO_2-H_2S co-injection cases. However, the brittleness of the limestone and sandstone rocks decreased significantly for the CO_2-SO_2 co-injection case (while the brittleness of the carbonate rock initially composed on calcite and dolomite minerals varies vertically in the formation).

6. Shale formations are preferable cap rocks, as their brittleness decreases during CO_2 geosequestration at low or high temperature conditions. Carbonate formations might be suitable reservoirs for cyclic injection and withdrawal of CO_2 due to increased chance of injectivity and productivity at the different zones of the reservoir; while sandstone formations are suitable reservoirs for long-term storage of CO_2 as they are more favourable for CO_2 mineral trapping.

5.2 Recommendations for Future Study

1. Future studies should consider performing experiments to determine changes in the mechanical strengths (compressive and tensile strengths) of rocks and their corresponding changes in the mechanical brittleness index of the rocks during CO_2 co-injection with H_2S or SO_2 gas.
2. Further studies should be conducted to incorporate data of molar volumes of minerals in the models developed in this study, to evaluate the brittleness index of carbonate, sandstone, and shale rocks before and after CO_2 sequestration (with or without H_2S/SO_2 gas).
3. Future studies should perform numerical simulations over thousands of years and determine the impact of mineral trapping of CO_2, with solubility and residual trapping mechanisms, on the brittleness of rocks.

Author credit statement

Efenwengbe Nicholas Aminaho: Conceptualization, Investigation, Methodology, Validation, Analyses, and Writing. **Mamdud Hossain:** Primary Supervisor. **Nadimul Haque Faisal:** Secondary Supervisor.

Declaration of competing interest

The authors declare that they have no known competing financial interests or personal relationships that could have appeared to influence the work reported in this paper.

Acknowledgements

The authors would like to acknowledge the flexible funding and partnership offered by the UK Carbon Capture and Storage Research Community (UKCCSRC). This project is jointly funded by the Robert Gordon University (Aberdeen) and UKCCSRC, and forms part of a PhD study at the Robert Gordon University (Aberdeen).

REFERENCES

Alam, M.M. et al. (2014). Petrophysical and rock-mechanics effects of CO_2 injection for enhanced oil recovery: Experimental study on chalk from South Arne field, North Sea. *Journal of Petroleum Science and Engineering*, 122, pp. 468–487.

AL-Ameri, W.A. et al. (2014). Effect of CO_2 Sequestration Period on the Mechanical Properties of Carbonate Aquifers. Paper SPE 171702-MS presented at the Abu Dhabi International Petroleum Exhibition and Conference held in Abu Dhabi, UAE, 10–13 November 2014.

AL-Ameri, W.A. et al. (2016). Long-term effects of CO_2 sequestration on rock mechanical properties. *Journal of Energy Resources Technology*, 138, pp. 1-9.

Aminu, M.D. et al. (2018) CO_2-brine-rock interactions: The effect of impurities on grain size distribution and reservoir permeability. *International Journal of Greenhouse Gas Control, 7*8, pp. 168-176.

Bolourinejad, P. and Herber, R. (2014) Experimental and modelling study of storage of CO_2 and impurities in a depleted gas field in northeast Netherlands. *Energy Procedia,* 63, pp. 2811-2820.

Dávila, G. et al. (2017) Experimental and modeling study of the interaction between a crushed marl caprock and CO2-rich solutions under different pressure and temperature conditions. *Chemical Geology*, 448, 26-42.

Edlmann, K. et al. (2013). Experimental investigation into the sealing capability of naturally fractured shale caprocks to supercritical carbon dioxide flow. *Environ Earth Sci*, 70, pp. 3393–3409.

Espinoza, D.N. and Santamarina, J.C. (2017). CO_2 breakthrough – Caprock sealing efficiency and integrity for carbon geological storage. *International Journal of Greenhouse Gas Control,* 66, pp. 218-219.

Ezema, I.C. et al. (2015). A Comperative Prediction of the Tensile Properties of Sisal Fiber Reinforced Epoxy Composite Using Volume Fraction and Mass Fraction Models. *Journal of Metallurgical and Materials Engineering Research*, 1 (2), pp. 9-18.

Fatah, A. et al. (2022). Geochemical modelling of CO2 interactions with shale: Kinetics of mineral dissolution and precipitation on geological time scales. *Chemical Geology*, 592, pp. 1-11.

Gong, Q.M. and Zhao, J. (2007). Influence of rock brittleness on TBM penetration rate in Singapore granite. *Tunn. Undergr. Space Technol*, 22 (3), pp. 317–324.

Guo, L. et al. (2016). Mineralogy and Shale Gas Potential of Lower Silurian Organic-Rich Shale at the Southeastern Margin of Sichuan Basin, South China. Oil Shale, 33 (1), pp. 1–17.

Hedayati, M. et al. (2018). Impacts of SO_2 gas impurity within a CO_2 stream on reservoir rock of a CCS pilot site: experimental and modelling approach. International Journal of Greenhouse Gas Control, 70, pp. 32–44.

Hou, B. et al. (2018). Brittleness Evaluation of Shale Based on the Brazilian Splitting Test. *Geofluids,* 2018, pp. 1-11.

Huang, Y. et al. (2018). The Effects of NaCl Concentration and Confining Pressure on Mechanical and Acoustic Behaviors of Brine-Saturated Sandstone. *Energies*, 11, 385, pp. 1-17.

Hucka, V. and Das, B. (1974). Brittleness Determination of Rocks by Different Methods. *Int. J. Rock Mech. Min. Sci. & Geomech*, 11, pp. 389-392.

Jin, X. et al. (2015). An Integrated Petrophysics and Geomechanics Approach for Fracability Evaluation in Shale Reservoirs. *SPE Journal,* 20 (3), pp. 518-526.

Kang, Y. et al. (2020). Mineralogical brittleness index as a function of weighting brittle minerals—from laboratory tests to case study. *Journal of Natural Gas Science and Engineering,* 77, pp. 1-9.

Khan, M.Y. and Mandal, A. (2020). Analytical model for gravity segregation in WAG displacement recovery of inclined stratified reservoirs. *Journal of Petroleum Science and* Engineering, 186, pp. 1-17.

Klokov, A. et al. (2017) Diffraction imaging for seal evaluation using ultra high resolution 3D seismic data. *Marine and Petroleum Geology*, 82, pp. 85-96.

Lasaga, A.C., Soler, J.M., Ganor, J., Burch, T.E. and Nagy, K.L. (1994). Chemical weathering rate laws and global geochemical cycles. *Geochimica et Cosmochimica Acta*, 58, pp. 2361-2386.

Li, C. et al. (2016). Effects of H_2S injection on the CO_2-brine-sandstone interaction under 21 MPa and 70 °C. *Marine Pollution Bulletin,* 106, pp. 17–24.

Li, G. (2016) Numerical investigation of CO_2 storage in hydrocarbon field using a geomechanical-fluid coupling model. *Petroleum*, 2, pp. 252-257.

Li, H. (2022). Research progress on evaluation methods and factors influencing shale brittleness: A review. Energy Reports, 8, pp. 4344–4358.

Liu, M. et al. (2014). Experimental studies on the short term effect of CO_2 on the tensile failure of sandstone. *Energy Procedia*, 63, pp. 3357 – 3363.

Liu, Y. et al. (2020) Investigation on mechanical behaviors of shale cap rock for geological energy storage by linking macroscopic to mesoscopic failures. *Journal of Energy Storage*, 29, pp. 1-15.

Liu, Y. and Dai, F. (2021). A review of experimental and theoretical research on the deformation and failure behavior of rocks subjected to cyclic loading. *Journal of Rock Mechanics and Geotechnical Engineering,* 13, pp. 1203-1230.

Luan, X. et al. (2014). Laboratory Measurements of Brittleness Anisotropy in Synthetic Shale with Different Cementation. Presented at the SEG Denver 2014 Annual Meeting.

Lyu, Q. et al. (2018). A Damage Constitutive Model for the Effects of CO_2-Brine-Rock Interactions on the Brittleness of a Low-Clay Shale. *Geofluids,* 2018, pp. 1-14.

Ma, X. et al. (2019). Geochemical modeling of changes in caprock permeability caused by CO_2–brine–rock interactions under the diffusion mechanism. *Oil & Gas Science and Technology - Rev. IFP Energies Nouvelles*, 74 (83), pp. 1-13.

Masoudi, R. et al. (2012). An Integrated Reservoir Simulation-Geomechanical Study on Feasibility of CO_2 Storage in M4 Carbonate Reservoir, Malaysia. Paper IPTC 15029 presented at the International Petroleum Technology Conference held in Bangkok, Thailand, 7–9 February 2012.

Mavhengere, P., Wagner, N. and Malumbazo, N. (2022). Influences of SO_2 contamination in long term supercritical CO_2 treatment on the physical and structural characteristics of the Zululand Basin caprock and reservoir core samples. *Journal of Petroleum Science and Engineering*, 215, pp. 1-15.

Meng, F. et al. (2015). Evaluation Methodology of Brittleness of Rock Based on Post-Peak Stress–Strain Curves. *Rock Mech Rock Eng*, 48, pp. 1787–1805.

Narasimhan, T.N. and Witherspoon, P.A. (1976). An integrated finite difference method for analyzing fluid flow in porous media. *Water Resour. Res., 12 (1), pp. 57-64.*

Palandri, J.L. and Kharaka, Y.K. (2004). A Compilation of Rate Parameters of Water-Mineral Interaction Kinetics for Application to Geochemical Modeling (No. Open File Report 2004-1068). US Geological Survey.

Pearce, J.K. et al. (2016) Reactivity of micas and cap-rock in wet supercritical CO_2 with SO2 and O2 at CO2 storage conditions. *Applied Geochemistry,* 72, pp. 59-76.

Pearce, J.K. et al. (2019) Geochemical modelling of experimental O_2–SO_2–CO_2 reactions of reservoir, cap-rock, and overlying cores. *Applied Geochemistry,* 109, pp. 1-19.

Pruess, K. (2004). The TOUGH Codes - A family of simulation tools for multiphase flow and transport processes in permeable media. *Vadose Zone Journal*, 3, pp. 738-746.

Rickman, R. et al. (2008). A practical use of shale petrophysics for stimulation design optimization: All shale plays are not clones of the Barnett Shale. In: Proceedings of the SPE Annual Technical Conference and Exhibition, Society of Petroleum Engineers.

Saraji, S. et al. (2013). Wettability of Supercritical Carbon Dioxide/Water/Quartz Systems: Simultaneous Measurement of Contact Angle and Interfacial Tension at Reservoir Conditions. *Langmuir,* 29, pp. 6856-6866.

Smith, S.A. et al. (2009) Geomechanical testing and modeling of reservoir and cap rock integrity in an acid gas EOR/sequestration project, Zama, Alberta, Canada. *Energy Procedia*, 1, pp. 2169–2176.

SNC-Lavalin Inc. (2004). Impact of Impurities on CO_2 Capture, Transport and Storage. IEA Greenhouse Gas R&D Programme Report (No. PH4/32).

Sobia, F. et al. (2021). An Experimental and Simulation Study of CO_2 Sequestration in Underground Formations: Impact on Geomechanical and Petrophysical Properties. Paper (SPE-204726-MS) presented at the SPE Middle East Oil & Gas Show and Conference, November 28–December 1, 2021.

Sun, Y. et al. (2016). Laboratory core flooding experimental systems for CO_2 geosequestration: An updated review over the past decade. Journal of Rock Mechanics and Geotechnical Engineering, 8, pp. 113-126.

Tariq, Z. et al. (2018). Geomechanical Studies on CO_2 Sequestrated Rocks in an Aqueous Saline Environment. Paper SPE 192242-MS presented at the Annual Technical Symposium & Exhibition held in Dammam, Saudi Arabia, 23–25 April 2018.

Tursic, J. et al. (2003). Influence of ionic strength on aqueous oxidation of SO_2 catalyzed by manganese. *Atmospheric Environment*, 37, pp. 2589–2595.

Wang, J. et al. (2022). CO_2 storage in carbonate rocks: An experimental and geochemical modeling study. *Journal of Geochemical Exploration,* 234, pp. 1-14.

Wei, X.C. et al. (2015) Uncertainty analysis of impact indicators for the integrity of combined caprock during CO_2 geosequestration. *Engineering Geology*, 196, pp. 37–46.

Wu, J. et al. (2019) Impact of pore structure and fractal characteristics on the sealing capacity of Ordovician carbonate cap rock in the Tarim Basin, China. *Marine and Petroleum Geology*, 102, pp. 557–579.

Xu, T. et al. (2006). TOUGHREACT: A simulation program for non-isothermal multiphase reactive geochemical transport in variably saturated geologic media. *Computer & Geosciences,* 32, pp. 145-165, DOI information: 10.1016/j.cageo.2005.06.014.

Xu, T. et al. (2014). TOUGHREACT V3.0-OMP Reference Manual: A Parallel Simulation Program for Non-Isothermal Multiphase Geochemical Reactive Transport.

Yeh, G.T. and Tripathi, V.S. (1991). A model for simulating transport of reactive multispecies components: model development and demonstration. *Water Resour. Res.*, 27, pp. 3075-3094.

Zhang, W., Xu, T. and Li, Y. (2010). Modeling of fate and transport of co-injection of H_2S with CO_2 in deep saline formations. United States. DOI: https://www.osti.gov/servlets/purl/1007193

Zhang, D. et al. (2016). The brittleness indices used in rock mechanics and their application in shale hydraulic fracturing: A review. *Journal of Petroleum Science and Engineering,* 143, pp. 158–170.

Zheng, L. et al. (2009). On mobilization of lead and arsenic in groundwater in response to CO_2 leakage from deep geological storage. *Chemical Geology*, 268, (3-4), pp. 281-297.

APPENDICES